

Vredenburg and colleagues<sup>4</sup> and Briggs *et al.*<sup>5</sup> carried out long-term, large-scale monitoring and sampling of amphibian populations in the Sierra Nevada in California, focusing on yellow-legged frogs — *Rana muscosa* and *Rana sierrae* — the populations of which have declined in recent decades. Previous studies focused exclusively on the prevalence of infection (that is, the proportion of infected hosts), ignoring the role of infection intensity (the amount of infection per individual host) in controlling host-population losses. Instead of simply cataloguing the presence or absence of *B. dendrobatidis* and its spread among host populations, these investigators<sup>4,5</sup> identify a 'lethal threshold' of pathogen infection intensity, which may be the key to understanding how *B. dendrobatidis* epidemics can be controlled.

Vredenburg *et al.*<sup>4</sup> carried out intensive sampling of 88 frog populations over 9–13 years. Among the lakes they studied, they found that, within three years of its arrival, *B. dendrobatidis* had spread in a wave-like pattern — that is, the area covered by the pathogen increased steadily in size over time — until nearly all of the frog populations at the lake were infected. The amphibian populations did not, however, collapse until a lethal threshold of about 10,000 zoospores of the fungus per frog was reached.

The existence of such an intensity threshold may help to explain how *B. dendrobatidis* causes almost complete losses of amphibian hosts. Because of this threshold, there is a time lag between exposure and mortality, so the pathogen can spread through much of the amphibian population before disease-driven reductions in host density negatively affect the transmission of *B. dendrobatidis*. Consequently, the pathogen can cause the loss and extinction of its host population, unlike the many other pathogens that disappear as their hosts decline in numbers.

Briggs *et al.*<sup>5</sup> combine long-term field data with modelling analysis to investigate how some amphibian populations persist even though *B. dendrobatidis* is present in their habitat. The authors' intensive data — involving marking the animals and later recapturing them — show that, in populations that survive, infected yellow-legged frogs have fungal loads well below the lethal intensity threshold, and that these frogs have cleared fungal infection and become reinfected over the course of years, with no effect on their survival.

Previous studies suggested that genetic changes that alter host tolerance of the pathogen or pathogen virulence might explain how some amphibian populations persist in the presence of *B. dendrobatidis*. Briggs and colleagues' modelling efforts, however, hint that simple decreases in host density and the resultant reduction in pathogen transmission could account for such an outcome. This is particularly true when there are environmental reservoirs of *B. dendrobatidis*, including amphibian species or life stages (such as tadpoles) that can persist with the infection for long periods

and spread it to more sensitive hosts.

This modelling work<sup>5</sup>, which was based on a variety of biological scenarios, offers insight into both the epidemic and endemic aspects of *B. dendrobatidis* dynamics. For instance, the study predicts that infection intensity builds up rapidly when frog populations are dense, as well as under conditions that promote reinfection. If *B. dendrobatidis* reaches its intensity threshold, the infected amphibian population can become extinct. By contrast, if some members of the host population survive, then a new endemic state develops, with persistent infection in the remaining frogs.

Intriguingly, both studies<sup>4,5</sup> indicate that the traditional dichotomous classification of pathogens as either microparasites or macroparasites may be overly simplistic, as the dynamics of infection with *B. dendrobatidis* — a microparasite — strongly depend on infection intensity (which is usually considered only for macroparasites). This finding suggests that incorporating infection intensity into other microparasite disease models could provide insight into other host–pathogen systems.

The new papers<sup>4,5</sup> markedly increase the understanding of a disease that affects many amphibian populations. In particular, the types of data presented — based on long-term, extensive monitoring that generates detailed records — are largely unprecedented for analyses of many wildlife disease systems.

Nevertheless, large gaps remain in the knowledge of *B. dendrobatidis* and in how the dynamics of chytridiomycosis vary between geographical regions. The populations that these researchers<sup>4,5</sup> studied are from montane ecosystems that have low species diversity and relatively harsh winter conditions. Will the reported dynamics for *B. dendrobatidis* in this system explain the spread of this pathogen in, for example, lowland regions of Europe or in the tropics, where host-species density is substantially higher?

Moreover, it is still not clear precisely which vectors spread the infection, in which systems it is endemic and in which ones it is epidemic, and whether environmental changes can

trigger the emergence of this pathogen. By focusing on infection intensity and the differences between epidemic and endemic states of *B. dendrobatidis* infection, Vredenburg *et al.* and Briggs *et al.* lay a valuable foundation for addressing questions such as how the intensity threshold of *B. dendrobatidis* varies across species or with environmental conditions, and what part is played by environmental cofactors such as climate change<sup>8</sup> in affecting the dynamics of endemic infection.

How can this information be applied so as to slow, or even prevent, population declines? As the authors of both papers propose, interventions designed to prevent *B. dendrobatidis* infection from reaching the lethal-intensity threshold could reduce extinction events. Because it is unlikely that the pathogen will be completely eradicated, the only realistic option may be to manage sensitive amphibian populations in such a way as to create an endemic state of infection. For instance, as described in a News Feature in these pages last week<sup>9</sup>, reducing the density of susceptible frogs by capturing them before the infection wave, or by treating a subset of individuals with an antifungal agent, could reduce transmission of *B. dendrobatidis* and prevent infection intensities from becoming lethal. ■

Andrew R. Blaustein is in the Department of Zoology, 3029 Cordley Hall, Oregon State University, Corvallis, Oregon 97331-2914, USA. Pieter T. J. Johnson is in the Department of Ecology and Evolutionary Biology, N122, CB334 University of Colorado, Boulder, Colorado 80309-0334, USA.  
e-mails: blaustea@science.oregonstate.edu; pieter.johnson@colorado.edu

1. Stuart, S. N. *et al. Science* **306**, 1783–1786 (2004).
2. Blaustein, A. R. & Kiesecker, J. M. *Ecol. Lett.* **5**, 597–608 (2002).
3. Daszak, P., Cunningham, A. A. & Hyatt, A. D. *Divers. Distrib.* **9**, 141–150 (2003).
4. Vredenburg, V. T., Knapp, R. A., Tunstall, T. S. & Briggs, C. J. *Proc. Natl Acad. Sci. USA* **107**, 9689–9694 (2010).
5. Briggs, C. J., Knapp, R. A. & Vredenburg, V. T. *Proc. Natl Acad. Sci. USA* **107**, 9695–9700 (2010).
6. Voyles, J. *et al. Science* **326**, 582–585 (2009).
7. Blaustein, A. R. *et al. Conserv. Biol.* **19**, 1460–1468 (2005).
8. Pounds, J. A. *et al. Nature* **439**, 161–167 (2006).
9. Lubick, N. *Nature* **465**, 680–681 (2010).

## STRUCTURAL BIOLOGY

# Immunity takes a heavy Toll

Steven A. Wasserman

**Toll receptors trigger immune responses through adaptor proteins and kinase enzymes. Structural studies reveal that hierarchical assembly of these proteins into a helical tower initiates downstream signalling events.**

Communication within cells often involves a series of molecular handshakes, each protein contacting the next and modifying its activity. An accessory protein may serve as a matchmaker, holding components together for

the exchange of information. Until now, this model fitted well with what was known about signalling in mammalian Toll pathways, which activate innate immune defences<sup>1</sup>. Three proteins — MyD88 and two members of the IRAK

protein family — help to link pathogen recognition by transmembrane Toll receptors to the transcription of genes involved in defence. MyD88 and the IRAKs each contain a single death domain, a region that allows their interaction with the death domain of other proteins. But as Wu and colleagues (Lin *et al.*<sup>2</sup>) report on page 885 of this issue, the death domains do not form a simple chain. Rather, their X-ray crystal structure reveals that the death domains from several copies of each protein combine into a signalling tower more than 100 ångströms high.

Death domains were discovered and so named for their role in apoptosis, a form of programmed cell death. They were later found in components of signalling pathways governing immunity and inflammation. Disruption of signalling pathways by these domains contributes to cancer and a wide range of inflammatory disorders<sup>3</sup>.

Built from six  $\alpha$ -helices, death domains have three noteworthy characteristics<sup>4</sup>. First, their interaction is homotypic — that is, death domains bind only to other death domains. Second, this interaction can take three forms (I–III) that differ at their contact sites and that each lacks mirror-image symmetry. And third, the amino-acid sequence of these domains is highly variable, with the sequences of distantly related death domains differing by 90%.

The structure that Lin *et al.*<sup>2</sup> solve is the first to contain death domains from three different proteins. Here, the death domains of six MyD88 molecules comprise the first two of four layers in the complex. Four IRAK4 death domains form the next layer, and four domains from IRAK2 complete the structure (Fig. 1). Because the layers form at a slight tilt, the final shape is a left-handed helical tower. Type I and II interactions are found exclusively between layers, whereas type III interactions connect adjacent death domains along the spiral. The net effect is a cylindrical honeycomb with hexagonally arrayed protein–protein contacts.

How could an infection trigger assembly of this death-domain complex? Each cell-surface Toll protein acts as a sentinel for invading viruses and microorganisms: its extracellular portion binds to molecules found in microbes but not in animal cells, such as cell-wall components. The intracellular portion of these receptors has a TIR domain, which can interact with other TIR domains. Binding of a pathogen molecule to Toll receptors induces their dimerization by bringing together their TIR domains. The clustering of TIR domains, in turn, generates a binding site for MyD88, which also has a TIR domain. The Toll–MyD88 interaction raises the local concentration of MyD88 enough to initiate assembly of the signalling complex. Because self-association of MyD88 is quite weak, Toll activation is also required for MyD88 oligomerization and thus complex formation.

Combining structural data with the technique of site-directed mutagenesis, Lin and

colleagues<sup>2</sup> demonstrate that recruitment of each IRAK4 molecule to the nascent complex involves multiple points of contact with other death domains. Addition of IRAK2 then follows to complete the hierarchical assembly process. But what prevents IRAK2 from joining earlier, and why does assembly stop at four layers? To answer these questions, the authors quantitated the extent to which the surfaces of each of the three death domains are complementary in charge and shape. These calculations reveal that the interactions of IRAK4 with MyD88 and with IRAK2 are sufficiently distinct to provide a fixed order for assembly.

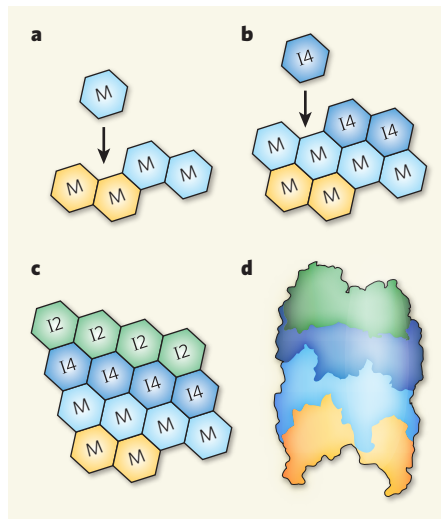


**Figure 1 | Signalling-complex assembly in the Toll pathway.** **a–c**, Assembly of the death-domain complex (viewed as if split along a roughly vertical seam and laid flat). Assembly begins when pathogen-induced dimerization of Toll recruits MyD88 molecules through TIR-domain interactions (not shown). Clustering of the MyD88 death domains (M) induces the formation of the first two layers of the signalling complex. MyD88 death domains provide composite binding sites for IRAK4 death domains (I4), which in turn recruit IRAK2 (I2). **d**, Structure of the completed signalling tower. The kinase domains of IRAK4 and IRAK2 (not shown) lie on the outside of this complex.

Lin *et al.* further show that the top and bottom surfaces of IRAK2 are incompatible with one another, preventing inclusion of extra IRAK2 molecules in the finished tower.

Once the signalling complex has formed, the IRAKs undergo phosphorylation<sup>5</sup>. Both IRAK4 and IRAK2 are protein kinases — phosphorylating enzymes. The immediate consequence of complex formation is IRAK4 autocatalysis. Autophosphorylated IRAK4 then phosphorylates and activates IRAK2. Activated IRAK2 leaves the complex, initiating a cascade of protein modification and destruction — through ubiquitylation, phosphorylation and proteolysis — involving other protein complexes<sup>1</sup>. At the end, destruction of an inhibitor protein, I $\kappa$ B, frees the transcription factor NF- $\kappa$ B to enter the nucleus and direct the expression of

genes mediating immune responses.

The MyD88–IRAK4–IRAK2 complex is a key mediator of Toll signalling in humans: of the ten Toll receptors, all but one can signal through MyD88 (ref. 1). Furthermore, the activity of IRAK4 is essential for responses transduced by MyD88. IRAK4 in turn signals through IRAK2 or a closely related protein kinase, IRAK1 (ref. 5). Because the sites that contact IRAK4 are evolutionarily conserved between IRAK2 and IRAK1, Lin *et al.*<sup>2</sup> suggest that IRAK1 can substitute for IRAK2 in the signalling tower. This raises the question of whether IRAK1 and IRAK2, which have overlapping but distinct functions, are ever recruited into the same signalling tower.

The immune function of the Toll pathway has been conserved from fruitflies to humans<sup>6,7</sup>. Is the architecture of the signalling complex similarly conserved? The answer seems to be yes and no. In the fruitfly *Drosophila*, the counterparts<sup>8</sup> to MyD88, IRAK4 and IRAK2 are called MyD88, Tube and Pelle. From detailed structural analysis<sup>9</sup>, interaction between the Tube and Pelle death domains matches that between IRAK4 and IRAK1 to a high degree. Furthermore, key interactions between these two sets of proteins, mapped by inactivating mutations in the fly proteins, are evolutionarily conserved. However, studies in solution indicate<sup>10</sup> that the death domains of MyD88, Tube and Pelle form a ternary complex rather than a higher-order assembly.

Given that a death-domain trimer suffices for Toll signalling in *Drosophila*, why does the mammalian pathway have such an elaborate architecture? Lin and co-workers suggest that a helical symmetry more readily accommodates a variable number of specific binding partners. If so, helical complexes may be found in pathways for some of the other 84 human proteins that contain the six-helical-bundle characteristic of death domains. These superfamily members participate in cell death, inflammation, DNA-damage responses, detection of intracellular pathogens and antiviral immunity<sup>3</sup>. Structural studies of these pathways will reveal whether other death-domain proteins also gather at their respective receptors as a flock of signals. ■

Steven A. Wasserman is in the Section of Cell and Developmental Biology, University of California, San Diego, La Jolla, California 92093-0349, USA. e-mail: stevenw@ucsd.edu

1. Kawai, T. & Akira, S. *Trends Mol. Med.* **13**, 460–469 (2007).
2. Lin, S.-C. *et al.* *Nature* **465**, 885–890 (2010).
3. Gaestel, M., Kotlyarov, A. & Kracht, M. *Nature Rev. Drug Discov.* **8**, 480–499 (2009).
4. Park, H. H. *et al.* *Annu. Rev. Immunol.* **25**, 561–586 (2007).
5. Kawagoe, T. *et al.* *Nature Immunol.* **9**, 684–691 (2008).
6. Belvin, M. P. & Anderson, K. V. *Annu. Rev. Cell Dev. Biol.* **12**, 393–416 (1996).
7. Lemaître, B. & Hoffmann, J. *Annu. Rev. Immunol.* **25**, 697–743 (2007).
8. Towb, P., Sun, H. & Wasserman, S. A. *J. Innate Immun.* **1**, 309–321 (2009).
9. Xiao, T. *et al.* *Cell* **99**, 545–555 (1999).
10. Moncrieffe, M. C., Grossmann, J. G. & Gay, N. J. *J. Biol. Chem.* **283**, 33447–33454 (2008).



## Helical signaling complex

MyD88, IRAK4 and IRAK2 are involved in mediating signaling downstream of the Toll-like receptor (TLR) family (TLR/IL-1R). Toll-like receptors have critical roles in immune system signaling and during early development. They contain a common intracellular Toll/IL-1R homology (TIR) domain and, upon activation, recruit adaptors such as MyD88 that also contain TIR domains. MyD88 responds to most TLRs and contains a death domain that interacts with death domains on IRAK2 and IRAK4, eventually resulting in the activation of transcription factors, including NF- $\kappa$ B. Wu and colleagues have now solved the structure of a complex consisting of death domains from MyD88, IRAK4 and IRAK2, and found that they unexpectedly form a left-handed helical assembly. The complex consists of six MyD88, four IRAK4 and four IRAK2 subunits. Although this is a complex of all death domains, there is specificity to these interactions and thus ordering of the superhelical assembly, endowed by specific features contributed by the different subunits. Indeed, there are specific interactions between layers of MyD88, IRAK4 and IRAK2 in the helical assembly. Given homology to *Drosophila melanogaster* components involved in body axis patterning during embryogenesis and in innate immunity, the authors were able to construct a model of the assembly that might be involved in *Drosophila* developmental and innate immunity signaling. Together, these findings indicate that an unexpected versatile, yet conserved, assembly process may be triggered by signal transduction in this system. (*Nature* 465, 885–890, 2010) *SL*



GMP in the predivision stalk cell. Upon formation of the septum, an increase in the c-di-GMP levels in the stalk daughter and a marked decrease in the swarmer cell resulted in 5-fold differences in the sister cells. Mutation of *pleC* and *pleD* genes or overexpression of another diguanylate cyclase demonstrated the role of these enzymes in generating this asymmetrical c-di-GMP distribution, whose disruption resulted in abnormal motility phenotypes in the daughter cells. Such a pattern of c-di-GMP distribution in daughter cells was observed in *Pseudomonas aeruginosa* (which has a single polar flagellum) but also in bacteria with flagella distributed all around the cell (*Salmonella enterica*) or nonflagellated bacteria (*Klebsiella pneumoniae*), indicating that c-di-GMP likely regulates other asymmetrical cellular properties besides motility. (*Science* 328, 1295–1297, 2010) *IC*

## Nrde inhibition

Small RNAs are involved in the silencing of gene expression in many species, and previously, a genetic screen for mutants affecting RNA interference (RNAi) in *Caenorhabditis elegans* nuclei was conducted. Now Kennedy and colleagues have followed up on one set of alleles that define *nrde-2*. Mutations in *nrde-2* affect the silencing of nuclear RNAs, with *nrde-2* worms failing to show the Muv phenotype that arises upon *lin-15b* RNAi. *nrde-2* alleles were also shown to act in the same pathway as *nrde-3*, previously defined as a nuclearly localized Argonaute homolog required for silencing of nuclear transcripts. Through further analysis, it was found that *nrde-2* functions downstream of *nrde-3*-siRNA interaction as well as downstream of recruitment of NRDE-3 to the target messenger RNA. The authors find that *nrde-2* alleles map to a conserved factor containing a domain of unknown function (DUF) and Ser-Arg repeats as well as half-a-tetratricopeptide-like domain. These domains are found in RNA-processing factors and NRDE-2 localizes to the nucleus, but it is currently unclear exactly how NRDE-2 functions. However, through a further screen, the authors do find that *nrde-2* genetically interacts with a subunit of the RNA polymerase, Rbp7. Although it is not yet clear that Rbp7 is involved in RNAi, both NRDE-2 and NRDE-3 interact with pre-mRNAs, hinting at a co-transcriptional function. In addition, chromatin immunoprecipitation (ChIP) analysis indicates an increase in the methylation of histone H3 Lys9 that is *nrde-2* dependent, indicating an effect on chromatin. Using a nuclear run-on assay in *C. elegans* nuclei, the authors show that transcriptional elongation at the *lin-15b* locus was affected during *lin-15b* RNAi and that this effect was dependent on NRDE-2. Further investigation will elucidate the mechanism of silencing in this system as well as whether *nrde-2* and *nrde-3* are directly involved, and it will be interesting to see whether the homologs of *nrde-2* in other species are involved in a similar process. (*Nature*, published online 13 June 2010, doi:10.1038/nature09095) *SL*

## Heirloom messenger

*Caulobacter crescentus* is a bacterium that undergoes asymmetric cell division. The replication-competent cell is attached to a surface via a polar stalk and is thus termed the 'stalk cell'. Upon DNA replication and cell division, two different daughter cells arise, a stalk cell and a swarmer cell, the latter of which has a flagellum in the distal pole and can swim away. In *Caulobacter* and other bacteria, cellular motility and adhesion are controlled by an intracellular messenger, cyclic diguanosine monophosphate (c-di-GMP). Cellular levels of c-di-GMP are regulated by the action of multiple enzymes that synthesize or degrade this molecule (diguanylate cyclases and phosphodiesterases, respectively). The activity of such enzymes can be spatially restricted: for instance, the diguanylate cyclase PleD is inactivated in the *Caulobacter* swarmer cell due to the localization of an inactivating phosphatase, PleC, to the pole opposite the stalk in the predivision stalk cell. Now work from Miller and colleagues reveals that c-di-GMP itself is distributed in a remarkably asymmetrical fashion in the *Caulobacter* progeny. By fusing c-di-GMP sensors to fluorescent proteins CFP and YFP, the authors were able to measure FRET values in live cells that could be converted into c-di-GMP levels. Time-lapse microscopy showed homogeneous levels of c-di-

Written by Inès Chen & Sabbi Lall

# Helical assembly in the MyD88–IRAK4–IRAK2 complex in TLR/IL-1R signalling

Su-Chang Lin<sup>1</sup>, Yu-Chih Lo<sup>1</sup> & Hao Wu<sup>1</sup>

**MyD88, IRAK4 and IRAK2 are critical signalling mediators of the TLR/IL-1R superfamily. Here we report the crystal structure of the MyD88–IRAK4–IRAK2 death domain (DD) complex, which surprisingly reveals a left-handed helical oligomer that consists of 6 MyD88, 4 IRAK4 and 4 IRAK2 DDs. Assembly of this helical signalling tower is hierarchical, in which MyD88 recruits IRAK4 and the MyD88–IRAK4 complex recruits the IRAK4 substrates IRAK2 or the related IRAK1. Formation of these Myddosome complexes brings the kinase domains of IRAKs into proximity for phosphorylation and activation. Composite binding sites are required for recruitment of the individual DDs in the complex, which are confirmed by mutagenesis and previously identified signalling mutations. Specificities in Myddosome formation are dictated by both molecular complementarity and correspondence of surface electrostatics. The MyD88–IRAK4–IRAK2 complex provides a template for Toll signalling in *Drosophila* and an elegant mechanism for versatile assembly and regulation of DD complexes in signal transduction.**

Toll-like receptors (TLRs) and receptors for pro-inflammatory cytokines IL-1 and IL-18 share a common Toll/IL-1R homology (TIR) domain in their intracellular region and belong to the TLR/IL-1R superfamily<sup>1,2</sup>. TLRs recognize pathogen-associated molecular patterns (PAMPs) to initiate protective immune responses<sup>3,4</sup>. The molecular pathways for these receptors are complex and their dysregulation is associated with many human diseases in the immune system such as inflammatory disorders<sup>5,6</sup>, autoimmune diseases<sup>7–10</sup> and allergy<sup>11</sup> as well as diseases beyond the immune system such as cancer<sup>12</sup>, insulin resistance<sup>13</sup>, atherosclerosis<sup>14,15</sup>, and painful neuropathy<sup>16</sup>.

Signal transduction is initiated by the approximation of the receptor TIR domains on binding of PAMPs and cytokines<sup>1</sup>. This leads to the recruitment of intracellular TIR-containing adaptors such as MyD88, TIRAP, TRIF (also known as TICAM1) and TRAM<sup>17</sup>. MyD88 is critical for signalling responses of IL-1, IL-18 and all TLRs except TLR3<sup>3,17–19</sup>. In addition to its C-terminal TIR domain, MyD88 contains an amino-terminal death domain (DD) and a short intermediate domain (ID). Through the DD, MyD88 interacts with IRAKs, including IRAK1, IRAK2, IRAK4 and IRAK-M, which are characterized by an N-terminal DD and a carboxy-terminal Ser/Thr kinase or kinase-like domain<sup>3,20,21</sup>. Eventually, the ensuing pathway activates transcription factors NF- $\kappa$ B (also known as NFKB), AP-1 and IRFs to elicit anti-pathogen responses and inflammation<sup>3,17,22</sup>. Targeted deletions in mice have identified IRAK1, IRAK2 and IRAK4 as essential positive players and IRAK-M as a critical negative regulator in the pathway<sup>23–26</sup>. In humans, inherited MyD88 and IRAK4 deficiencies cause recurrent, often life-threatening infections by pyogenic bacteria<sup>27,28</sup>.

## Structure determination

To elucidate the molecular basis of DD-mediated TLR/IL-1R signalling, we co-expressed DDs of MyD88 and IRAKs. MyD88 DD interacted with IRAK4 DD to form a binary Myddosome complex that eluted from a gel filtration column with a molecular mass of 135.4 kDa (0.5% error) as measured by multi-angle light scattering (MALS) (Supplementary Fig. 1). Furthermore, a ternary Myddosome complex that also contains IRAK2 DD was formed and eluted with an apparent molecular mass of ~180 kDa.

We crystallized the MyD88–IRAK4–IRAK2 DD complex and determined its structure at 3.4 Å resolution using several heavy atom derivatives that included Au, Hg, Pt, Se and Ta cluster (Supplementary Table 1 and Supplementary Fig. 2). Because the IRAK4 DD structure is known<sup>29</sup>, we used it as a model to identify 14 DD structures in the experimental electron density map. We then distinguished the DD molecules as MyD88, IRAK4 and IRAK2 using the Se positions (Supplementary Table 2). The final atomic model comprises 6 MyD88, 4 IRAK4 and 4 IRAK2 DD molecules. The observed stoichiometries in the crystal agree well with the measured and apparent molecular masses of the binary MyD88–IRAK4 and the ternary MyD88–IRAK4–IRAK2 complexes (Supplementary Discussion 1), the gross staining intensities of the DDs in the complexes on SDS–PAGE (Supplementary Fig. 3) and a previous study showing the 6:4 stoichiometry when the MyD88–IRAK4 complex became slightly ‘stripped’ under a mild mass spectrometry condition<sup>30</sup>.

## Overall structure of the complex

The ternary Myddosome complex forms a tower-shaped structure about 110 Å in height and 70 Å in diameter (Fig. 1a). It contains approximately four layers, with MyD88 at the bottom two layers, IRAK4 in the middle layer and IRAK2 at the top layer. The centre of the MyD88 layers has a sizable cavity (Supplementary Fig. 4), in agreement with the prominent depression in the electron microscopy structure of the MyD88–IRAK4 complex<sup>30</sup>.

The six helical bundle structures<sup>31</sup> of MyD88, IRAK4 and IRAK2 DDs containing helices H1 to H6 each have their distinct features (Fig. 1b) with MyD88 being the most dissimilar (Supplementary Table 3). MyD88 has a short H3 and an extraordinarily long H6 from residue 99 to the end of the construct at residue 117, which includes part of the intermediate domain (ID, residues 110–154). MyD88s, a splice variant of MyD88 that does not contain the ID, did not interact with IRAK4 nor activate NF- $\kappa$ B<sup>32,33</sup>. Our structure indicates that the DD boundary of MyD88 does not end until about residue 117 and deletion of the MyD88 ID would result in a truncated DD. For the loop regions, MyD88 has the longest H1–H2 loop, shortest H3–H4 loop and the longest H4–H5 loop, and IRAK4 has the longest H2–H3

<sup>1</sup>Department of Biochemistry, Weill Cornell Medical College, New York, New York 10021, USA.

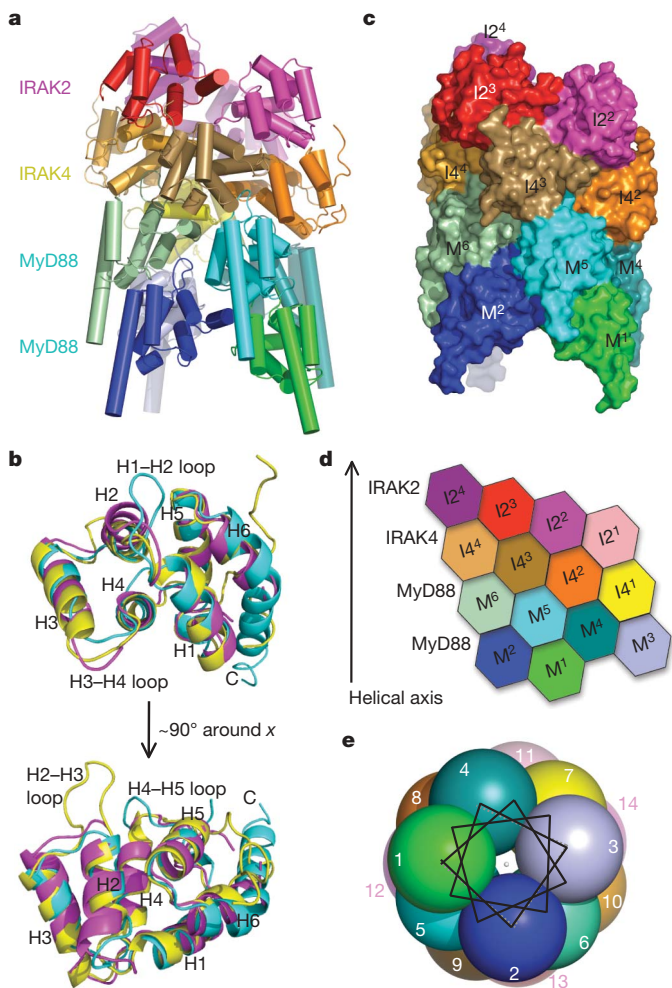


**Figure 1 | Structure of the ternary Myddosome complex.** **a**, Ribbon diagram of the structure, with the six MyD88 molecules in cold colours, the four IRAK4 molecules in earth-tone colours and the four IRAK2 molecules in warm colours. **b**, Superposition of MyD88 DD (cyan), IRAK4 DD (yellow) and IRAK2 DD (magenta). Helices H1 to H6 and the H1–H2, H2–H3 and H4–H5 loops are labelled. **c**, Surface diagram of the complex with each subunit labelled using the same colour coding as in **a**. M, MyD88; I4, IRAK4; I2, IRAK2. **d**, Planar arrangement of the complex. **e**, The helical symmetry is shown in a helical wheel representation with each ball representing a molecule and looking down the helical axis. Each molecule is labelled as an integer sequentially from M<sup>1</sup> to I2<sup>4</sup>.

loop. The MyD88 structure explains the disruptive phenotypes of mutations  $\Delta$ E52 and L93P in children suffering from life-threatening pyogenic bacterial infections<sup>28</sup> (Supplementary Fig. 5).

### The ternary complex forms a helical oligomer

To our surprise, the MyD88–IRAK4–IRAK2 complex is a single stranded left-handed helix of DDs, starting from the six molecules of MyD88 (M<sup>1–6</sup>), continuing with the four molecules of IRAK4 (I4<sup>1–4</sup>) and ending with the four molecules of IRAK2 (I2<sup>1–4</sup>) (Fig. 1c, 1d). In the helical oligomer, the adjacent individual DD molecules are related by a rotation of  $98 \pm 2^\circ$  and a translation along the helical axis of about 6 Å. This approximate helical symmetry provides a quasi-equivalent environment for each DD molecule in the ternary complex. The DD molecules complete almost four turns, with approximately 3.7 DD molecules per turn.

If we cut open the structure from the side and lay the molecules flat, the locations of the DDs form a staggered hexagonal pattern (Fig. 1d). Each molecule has maximally six immediate neighbouring DDs in this two-dimensional representation. This remains true even in the rolled up three-dimensional structure, because a given DD has

limited contacts with DDs beyond its immediate vicinity. The helical assembly can also be represented in a similar helical wheel used to show amphipathic  $\alpha$ -helices in protein structures (Fig. 1e). The nature of a helical assembly dictates that molecules at either ends of the helix are less ordered or perhaps exhibit less occupancy than the central molecules. This can be shown by the temperature factor distribution in the ternary complex (Supplementary Fig. 6).

### Composite binding sites and interaction specificity

The interactions in the helical assembly can be classified into three types. Type I and type II mostly mediate interactions between the layers, whereas type III represents contacts between adjacent DD molecules in the helical spiral (Fig. 2a–e and Supplementary Fig. 7). Superposition of the three type I interaction pairs, MyD88–MyD88, MyD88–IRAK4 and IRAK4–IRAK2, showed that they are highly similar to one another (Supplementary Fig. 8). Likewise, the three kinds of type II interaction pairs and the five kinds of type III interaction pairs superimpose well (Supplementary Fig. 8). The type I interaction is formed by H2 and H3 on one DD and H1 and H4 region on the other DD. The type II interaction is formed from two opposite edges of the DDs, centred around the H4–H5 loop on one DD and around the H1–H2 loop on the other DD. The type III interaction is formed between H3 of one DD and an edge of the other DD composed of the H1–H2 and H3–H4 loops. The type I and type II interactions are more extensive in buried surface areas than the type III interaction (Supplementary Fig. 7).

During signalling, MyD88 molecules are first recruited to activated receptors and oligomerized. This then forms the ‘seeds’ for inducing assembly of the complex. Recruitment of a downstream molecule requires direct interaction with the composite binding site of three molecules via all three types of interactions, type II with an  $n^{\text{th}}$  molecule, type I with an  $(n + 1)^{\text{th}}$  molecule and type III with an  $(n + 3)^{\text{th}}$  molecule (Fig. 2a). For example, the first IRAK4 molecule (I4<sup>1</sup>) interacts with three MyD88 molecules (M<sup>3</sup>, M<sup>4</sup> and M<sup>6</sup>) simultaneously during its recruitment (Fig. 2b, c), explaining the requirement of MyD88 oligomerization in signal-dependent IRAK4 recruitment. We confirmed the importance of all three sites in this IRAK4–MyD88 interaction using structure-based mutagenesis, which identified R12, V16, R20, E69, T76 and N78 of IRAK4 (Supplementary Fig. 9a, b), and V43, A44, E52, Y58, I61 and R62 of MyD88 (Supplementary Fig. 9a, c) as critical residues. The importance of MyD88 residues E52 and Y58 is consistent with previous mutational studies of MyD88 in IRAK4 recruitment and NF- $\kappa$ B signalling<sup>34</sup>. Similarly, recruitment of the first IRAK2 molecule would require interaction with the composite binding site of three IRAK4 molecules (I4<sup>1</sup>, I4<sup>2</sup>, I4<sup>4</sup>) through type I, II and III interfaces (Supplementary Fig. 9a, d, e). The importance of these sites in the IRAK2–IRAK4 interaction was also confirmed by structure-based mutagenesis, which identified Y6, W62, M66 and R67 of IRAK2 (Supplementary Fig. 9d) and F25, Q50, F51, R54 and A95 of IRAK4 (Supplementary Fig. 9e) as critical residues.

The IRAK4–MyD88 and the IRAK2–IRAK4 interactions are quite different, providing the specificity in Myddosome formation. At the MyD88–IRAK4 interface, the uniquely long H1–H2 loop of MyD88, including residues V43 and A44, interacts with R47, Y48, H52, D73 and T76 of IRAK4 (Fig. 2b, c and Supplementary Fig. 7). There is no such corresponding interaction between IRAK2 and IRAK4. At the IRAK2–IRAK4 interface, there is a reciprocal interdigitation of the surfaces. Y6, W62 and M66 of IRAK2 insert into a region surrounded by F25, P28, Q29, Q50, R54, E92, F94, A95 and P96 of IRAK4. Conversely, Q50 and R54 of IRAK4 insert into a region surrounded by I5, Y6, L8, S10, L13, R58, E59 and W62 of IRAK2 (Fig. 2d, e and Supplementary Fig. 7). The equivalent inserted residues at the IRAK4–MyD88 interface are R12, F72 and T76 of IRAK4 and Y58 and R62 of MyD88, which are not only different but also much less interdigitating in the interaction.

The specificity in Myddosome formation may also be elucidated from analysis of the surface charge and shape complementarity



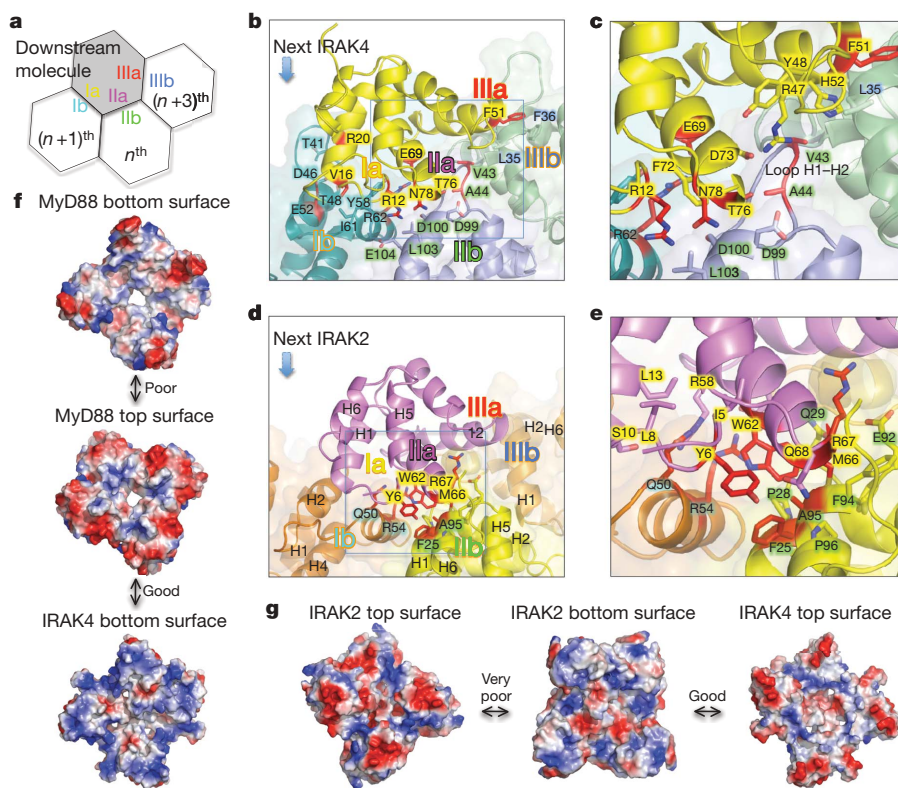


**Figure 2 | Composite interactions and specificity in the ternary complex.** **a**, Schematic representation of a composite binding site. The  $n^{\text{th}}$ ,  $(n+1)^{\text{th}}$  and  $(n+3)^{\text{th}}$  molecules provide type IIb, Ib and IIIb surfaces to interact with the type Ila, Ia and IIIa surfaces of a downstream molecule, respectively. **b**, Composite binding site for IRAK4 (yellow) formed from three MyD88 molecules ( $M^3$ ,  $M^4$  and  $M^6$ ) through type I, II and III interactions. **c**, Enlargement of the square in **b**. Note that the unique H1–H2 loop of MyD88 is critical for Myddosome assembly. **d**, Composite binding site for IRAK2 (purple) formed from three IRAK4 molecules ( $I^1$ ,  $I^2$  and  $I^4$ ) through type I, II and III interactions. **e**, Enlargement of the square in **d**. **f**, Good charge complementarity between IRAK4 and MyD88 and poor charge complementarity between the top and bottom surfaces of MyD88. **g**, Good charge complementarity between IRAK2 and IRAK4 and very poor charge complementarity between the top and bottom surfaces of IRAK2.

between the layers of DD molecules. Inspection of the top and bottom surfaces of MyD88 layers indicated that the charge complementarity between these surfaces is weak (Fig. 2f). In addition, the shape complementarity scores (Sc, ref. 35) between MyD88 DDs (such as the type II and type III interactions) are in the range of 0.3 and 0.4, the lowest among all the interactions in the complex (Supplementary Fig. 7). The relatively poor charge and shape complementarity may explain the observed variable stoichiometry of MyD88 in the binary Myddosome complex<sup>30</sup> (Supplementary Discussion 1).

In contrast to the weak complementarity between the top and bottom surfaces of MyD88, the bottom surface of IRAK4 matches well with the top surface of MyD88 both in charge complementarity (Fig. 2f) and in shape complementarity as shown in the Sc scores (Supplementary Fig. 7). The top surface of IRAK4 has good charge complementarity (Fig. 2g) and shape complementarity (Supplementary Fig. 7) with the bottom surface of IRAK2, resulting in specific recruitment of IRAK2. Because of the incompatibility between the top and bottom surfaces of IRAK2, only one layer of IRAK2 can assemble into the helical oligomer (Fig. 2g).

### Hierarchical and sequential assembly

Our reconstitution experiments indicated the presence of hierarchy in formation of the helical signalling tower in the Myddosome (Supplementary Fig. 10). MyD88 DD and IRAK4 DD formed a stable complex whereas IRAK2 DD did not form a stable complex with either MyD88 or IRAK4 alone. Instead, IRAK2 DD interacted with the MyD88–IRAK4 complex. These data support the concept that IRAK4 recruitment to MyD88 is an event upstream to IRAK2 recruitment in the TLR/IL-1R signalling pathways. IRAK1 DD did not express in any of our reconstitution experiments; however, previous data showed that IRAK4 and IRAK1 did not directly associate and that addition of MyD88 permitted assembly of a complex containing both IRAKs<sup>32,36</sup>. In the ternary complex, it has been shown that IRAK4 auto-phosphorylation occurs first and that IRAK4 activation is critical for IRAK1 and IRAK2 phosphorylation and activation<sup>36</sup>. In IRAK4-deficient mice, neither IRAK1 nor IRAK2 could be recruited to the TLR signalling complexes<sup>24</sup>. Whereas IRAK4 is absolutely

required for MyD88-dependent signalling<sup>24</sup>, IRAK1 and IRAK2 have somewhat redundant roles<sup>25</sup>. Our sequence alignment showed that IRAK2 residues critical for interaction with the MyD88–IRAK4 complex are conserved in IRAK1 (Supplementary Fig. 9a), confirming the biological observation.

It has been shown that in solution, MyD88 DD can form oligomers under a high protein concentration in a reversible manner<sup>30</sup> whereas IRAK4 DD is a monomer in solution. This indicates that when brought into proximity during TLR/IL-1R signalling, the weak MyD88 oligomer would be stabilized and acts as an initial platform for IRAK4 recruitment and subsequently IRAK1 and IRAK2 recruitment (Fig. 3a). In turn, IRAK4 recruitment further stabilizes the MyD88–IRAK4 complex, a notion supported by our mutagenesis results. The IRAK4 residue F25 participates in both type II interaction with IRAK2 and type III interaction with its neighbouring IRAK4. Unexpectedly, the F25D mutation not only impaired the ability of IRAK4 to pull down IRAK2, but also weakened the ability of IRAK4 to pull down MyD88 (Supplementary Fig. 9e), indicating that a stabilized type III interaction among IRAK4 DDs is important for Myddosome assembly. A most possible mode of DD assembly during signalling is a sequential assembly starting from clustered MyD88 then to IRAK4, then to IRAK2. The composite binding sites provided by the initial segments of the helical oligomer would provide a platform for concerted recruitment of IRAK4 and IRAK2 DDs, in a highly cooperative ‘chain’ reaction (Fig. 3a, Supplementary Discussion 2).

If we place the ternary Myddosome complex next to the TIR domains of TLR/IL-1-Rs with the C-terminal helices of MyD88 pointing towards the cellular membrane, the C-terminal TIR domains of MyD88 molecules would be poised to interact with clustered receptor TIR domains and other TIR-containing adaptors such as TIRAP (Fig. 3b). Given that four MyD88 molecules are minimally required to form one layer in the helical assembly, it is likely that dimerization of TLR/IL-1-Rs per se is not efficient for inducing signalling. It has been shown that TLRs can be recruited to lipid rafts on stimulation<sup>37</sup>, which would favour higher order receptor oligomerization to facilitate Myddosome assembly. The clustered IRAK4 kinase domains can

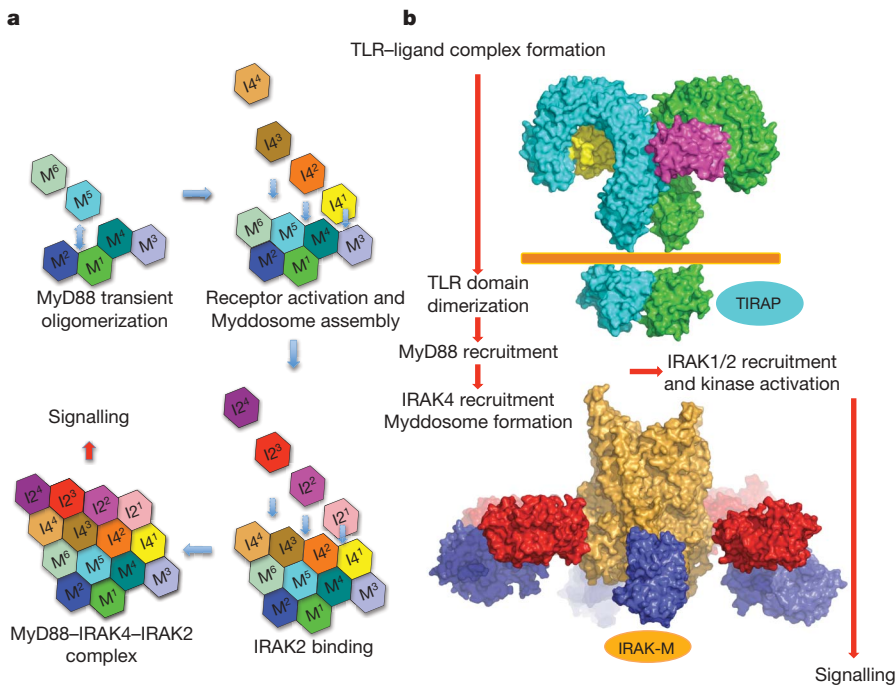


**Figure 3 | Model of sequential assembly in TLR/IL-1R signalling.** **a**, On ligand binding, TLR/IL-1Rs, including the cytoplasmic TIR domains, are dimerized or oligomerized. This results in the recruitment of other TIR containing adaptor proteins. In this case, MyD88 is recruited to the receptor complex and the death domain is oligomerized. In the presence of IRAK4, the death domain of IRAK4 ( $I4^1$ ) can be recruited to the oligomerized MyD88 DDs through the three interfaces ( $M^3$ ,  $M^4$ ,  $M^6$ ) and quickly forms the binary Myddosome complex. Downstream kinases (IRAK2 in this case, but IRAK1 as well) can then be recruited in a similar fashion and signalling is triggered. **b**, A model of the TLR signalling complex that recruits the MyD88–IRAK4–IRAK2 complex with proteins drawn to scale. TLRs, cyan and green (PDB code 3FXI for the extracellular domain of TLR4 and PDB code 2J67 for the TIR domain of TLR10). MD2, yellow and magenta (PDB code 3FXI in complex TLR4). Orange, MyD88–IRAK4–IRAK2 complex. Red, IRAK4 kinase domain (PDB code 2NRU). Blue, IRAK2 kinase domain using that of IRAK4.

then undergo auto-phosphorylation. In the crystal structure of the ternary complex, IRAK4 DDs and IRAK2 DDs pack closely against each other. The C-terminal tail of IRAK4 DD points towards the IRAK2 DD layer, whereas the C-terminal tail of IRAK2 DD points towards the IRAK4 DD layer. This arrangement would then bring the kinase domains of IRAK4 to the proximity of IRAK1 or IRAK2 to allow efficient phosphorylation by IRAK4 (Fig. 3b). These observations explain why a splice variant of IRAK1 that does not have an intact kinase domain<sup>38</sup> and two splice isoforms of IRAK2 that lack functional DDs<sup>39</sup> are negatively regulators in TLR/IL-1R signalling. It has been shown that once phosphorylated, IRAK1 or IRAK2 leaves the Myddosome and interacts with TRAF6 to elicit Lys63-linked polyubiquitination and downstream signalling<sup>40,41</sup>. We speculate that IRAK-M, a negative regulator of the TLR pathway, builds next to the IRAK2 layer of the ternary complex to prevent IRAK2 or IRAK1 dissociation and signalling.

### Implications on the dMyD88–Tube–Pelle complex

The mammalian TLRs are orthologues of the *Drosophila* Toll receptor, which is activated by the endogenous protein ligand Spätzle in response to microbial stimuli in immunity and spatial cues during embryonic development<sup>42</sup>. Intracellular signalling of Toll is mediated by dMyD88, Tube and the kinase Pelle<sup>43</sup>. A recent study suggested that Tube, although not having a kinase domain, is a homologue for the mammalian IRAK4 (ref. 44). A structural homology search using DALI<sup>45</sup> supports this conclusion because IRAK4 DD is most similar to Tube DD whereas IRAK2 DD is most similar to Pelle DD (Supplementary Table 4). Characterization of the DD interactions among these three *Drosophila* signalling proteins have also shown an unexpected parallel in the order of the assembly; formation of the dMyD88–Tube binary complex is the most stable ( $K_D = 1.2$  nM) and Pelle interacts much more preferentially with the dMyD88–Tube complex ( $K_D = 51$  nM) than with Tube alone ( $K_D = \sim 0.5$   $\mu$ M)<sup>46</sup>.

The organizational similarity prompted us to model the structure of the *Drosophila* Myddosome. Unlike the oligomeric MyD88–IRAK4–IRAK2 complex, the dMyD88–Tube–Pelle ternary complex in solution is 1:1:1 (ref. 46). Superposition of the known structure of the Tube–Pelle DD complex<sup>47</sup> onto a pair of type II IRAK4–IRAK2 interaction showed that they superimpose well with a slight orientational difference (Fig. 4a), indicating a conservation of this interaction between *Drosophila* and mammals. Superposition of Tube

DD with IRAK4 DD in a type II IRAK4–MyD88 interaction pair created a Tube–MyD88 complex that simulates the Tube–dMyD88 interaction. Combining this model with the structure of the Tube–Pelle complex created an elongated molecule with MyD88 and Pelle at either side of Tube (Fig. 4b). The shape of the ternary complex model is similar to the kidney shaped outline of the dMyD88–Tube–Pelle complex derived from small angle X-ray scattering (SAXS)<sup>46</sup>.

The validity of the ternary complex model is supported by published mutations R34E, K87E and R126E of Tube and D113K, D163K, D166K and D169K/D170K of dMyD88, that prevented interaction between Tube and dMyD88 (ref. 48). R34, K87 and R126 reside on the side of Tube modelled to interact with dMyD88, whereas D163, D166 and D169/D170 (equivalent to G97, D100 and L103/E104 of MyD88) are located on the surface of MyD88 modelled to interact with Tube (Fig. 4b, c). There is no equivalent of D113 of dMyD88 in MyD88 because it is located in a six-residue insertion in the already long H1–H2 loop, which directly interacts with Tube in the model. As in the IRAK4–MyD88 complex (Fig. 2f), there may also be charge complementarity in this Tube–dMyDD interface.

Notably, the structure of the Tube–Pelle complex shows a large surface burial of about 1,000  $\text{\AA}^2$  to allow 1:1 complex formation. This is provided by the C-terminal loop extension of Tube to enlarge the type II interface<sup>47</sup>. A similar situation may also apply to the Tube–dMyD88 interaction; Tube has a five-residue insertion in the H4–H5 loop and a long insertion in the H2–H3 loop that forms a pair of helices (H2' and H2'') in addition to the insertion in the H1–H2 loop of dMyD88 (Fig. 4b, c), all of which may increase the interaction surface and strength for the 1:1 complex formation. There is no direct interaction between dMyD88 and Pelle in our model of the complex, which is consistent with earlier biochemical studies<sup>46</sup>. It seems that a conformational change or a loss of entropy at the C-terminal loop extension of Tube may have been induced on dMyD88 interaction to enhance the ability of the dMyD88–Tube complex to interact with Pelle. In summary, *Drosophila* and mammals use a similar three-player system with different stoichiometry in Toll or TLR/IL-1R signalling. It is possible that on oligomerization of dMyD88 by activated Toll, an oligomeric form of the dMyD88–Tube–Pelle complex may be formed to allow auto-activation of the Pelle kinase. The apparent, higher complexity of the MyD88–IRAK4–IRAK2 complex may represent a more cooperatively controlled signalling system to accommodate the more complicated biology in mammals.



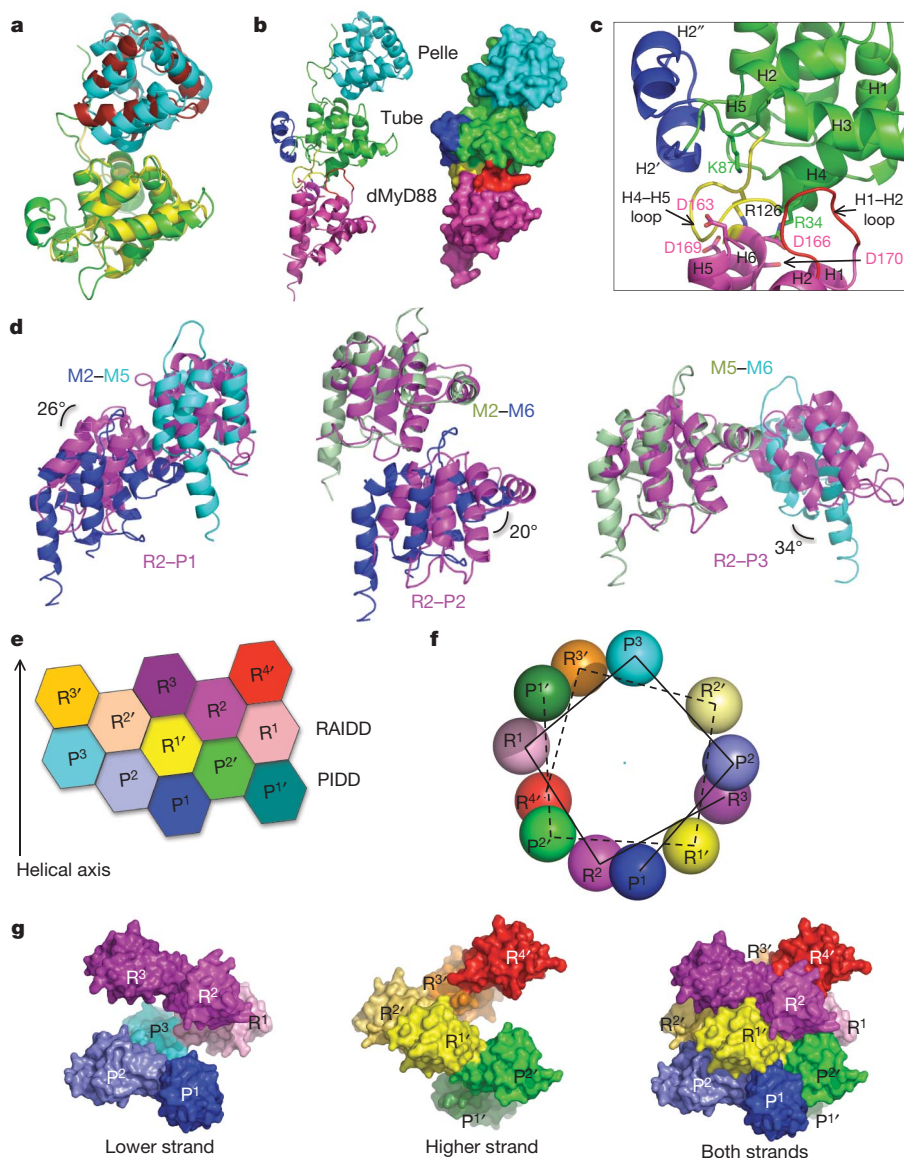


**Figure 4 | Common architecture in *Drosophila* Toll signalling and DD assembly in general.** **a**, Superposition of Tube–Pelle (green and cyan) and IRAK4–IRAK2 (yellow and brick red) complexes. **b**, Model of the dMyD88–Tube–Pelle complex in both ribbon and surface representations. Pelle is coloured in cyan. Tube is coloured in green except that the H2–H3 loop insertion (H2' and H2'') is in blue and the H4–H5 loop is in yellow. The model of dMyD88, obtained based on the MyD88 DD structure but without modelling the insertion in the H1–H2 loop, is coloured in magenta except that the H1–H2 loop is in red. **c**, Enlargement of the dMyD88–Tube interface. Residues important for dMyD88–Tube complex formation are shown in sticks. Note that the real H1–H2 loop of dMyD88 is six residues longer than that in the model. **d**, Superposition of the type I, II and III interactions in the MyD88–IRAK4–IRAK2 and the PIDD–RAIDD complexes. The resultant angular differences are labelled. **e**, Planar arrangement of the PIDD–RAIDD complex. R, RAIDD; P, PIDD. Subunits in one strand of the double helix are labelled as R and P and those in the other strand are labelled R' and P'. **f**, The helical symmetry is shown in a helical wheel representation with each ball representing a molecule and looking down the helical axis. Note that two helical strands are present in the complex. **g**, Surface representations of the two helical strands in the PIDD–RAIDD complex. The lower strand is about 5 Å lower than the higher strand, but they can be superimposed well. The lower strand (left) plus the higher strand (middle) equals the PIDD–RAIDD complex (right).

### Common helical oligomers for DD assembly

Comparison with the PIDD–RAIDD (p53-induced protein with a death domain–RIP-associated ICH-1 homologous protein with a death domain) complex that forms the core of the PIDDosome for caspase-2 activation<sup>19</sup> surprisingly showed that the three types of interfaces in the Myddosome are similar to those observed in the PIDD–RAIDD complex, despite the different apparent oligomerization schemes (Fig. 4d). Superposition of analogous interactions showed that the type I, II and III interactions differ by rotational differences of 25.8°, 19.9° and 34°, respectively. The conservation of the three types of interactions may be indicative of evolution of primordial DD interaction pairs as well as general match of shape concavity and convexity in these interfaces as dictated by the six helical bundle fold.

The MyD88–IRAK4–IRAK2 complex structure prompted us to re-inspect the structure of the PIDD–RAIDD complex. We discovered that the PIDD–RAIDD complex may be seen as a double stranded left-handed helical oligomer (Fig. 4e–g). One strand has three PIDD DD and three RAIDD DD molecules and the other strand contains two PIDD DDs and four RAIDD DDs, leading to the 5:7 stoichiometry of the PIDD DD–RAIDD DD complex. The relationship between a double-stranded and a single-stranded oligomer seems to be quite simple: when the two-dimensional representation is rolled up with one notch down, the arrangement turns from a double-stranded

oligomer to a single-stranded oligomer (Supplementary Fig. 11). This versatility explains how the PIDD–RAIDD complex and the MyD88–IRAK4–IRAK2 complex use similar interaction surfaces to create structures of different helical symmetries and stoichiometries.

A significant fraction of proteins in all kingdoms exists in the form of helical oligomers, which have been studied extensively by electron microscopy<sup>50</sup>. However, helical symmetry is rarely known in signal transduction. In the case of the MyD88–IRAK4–IRAK2 complex, the relative small size prevents detailed studies by electron microscopy and its tendency to be heterogeneous makes crystallization difficult. Yet helical symmetry seems to be especially suitable for regulating the pathway and the strength in signal transduction because complexes with helical symmetries can be evolved to accommodate variable number of binding partners with specificity. In addition, assembly of such complexes is sensitive to the number of receptors that are activated and the degree of their aggregation so that a threshold for eliciting complex formation can be set for the signalling processes. Many more signalling proteins may function as helical oligomers, including other DD superfamily members such as CARD, Pyrin and DED.

### METHODS SUMMARY

The DDs of human MyD88, IRAK4 and IRAK2 were co-expressed in *Escherichia coli* and co-purified by Ni-NTA affinity resin followed by gel filtration chromatography. Crystals grew at 20 °C at a protein concentration of about



1 mg ml<sup>-1</sup> using 50 mM Tris-HCl at pH 8.0, 100–250 mM MgCl<sub>2</sub>, and 8–15% ethanol.

**Full Methods** and any associated references are available in the online version of the paper at [www.nature.com/nature](http://www.nature.com/nature).

**Received 16 February; accepted 29 April 2010.**

**Published online 19 May 2010.**

- O'Neill, L. A. The interleukin-1 receptor/Toll-like receptor superfamily: 10 years of progress. *Immunol. Rev.* **226**, 10–18 (2008).
- Takeda, K., Kaisho, T. & Akira, S. Toll-like receptors. *Annu. Rev. Immunol.* **21**, 335–376 (2003).
- Akira, S., Uematsu, S. & Takeuchi, O. Pathogen recognition and innate immunity. *Cell* **124**, 783–801 (2006).
- Beutler, B. Inferences, questions and possibilities in Toll-like receptor signalling. *Nature* **430**, 257–263 (2004).
- Verstak, B., Hertzog, P. & Mansell, A. Toll-like receptor signalling and the clinical benefits that lie within. *Inflamm. Res.* **56**, 1–10 (2007).
- Marx, J. Biomedicine. Puzzling out the pains in the gut. *Science* **315**, 33–35 (2007).
- O'Neill, L. A. Primer: Toll-like receptor signaling pathways—what do rheumatologists need to know? *Nat. Clin. Pract. Rheumatol.* **4**, 319–327 (2008).
- Marta, M., Meier, U. C. & Lobell, A. Regulation of autoimmune encephalomyelitis by toll-like receptors. *Autoimmun. Rev.* **8**, 506–509 (2009).
- Lande, R. et al. Plasmacytoid dendritic cells sense self-DNA coupled with antimicrobial peptide. *Nature* **449**, 564–569 (2007).
- Pisitkun, P. et al. Autoreactive B cell responses to RNA-related antigens due to TLR7 gene duplication. *Science* **312**, 1669–1672 (2006).
- Horner, A. A. & Raz, E. Do microbes influence the pathogenesis of allergic diseases? Building the case for Toll-like receptor ligands. *Curr. Opin. Immunol.* **15**, 614–619 (2003).
- Chen, R. et al. Cancers take their Toll—the function and regulation of Toll-like receptors in cancer cells. *Oncogene* **27**, 225–233 (2008).
- Dasu, M. R., Devaraj, S., Park, S. & Jialal, I. Increased Toll-like receptor activation and TLR ligands in recently diagnosed type 2 diabetes subjects. *Diabetes Care* **33**, 861–868 (2010).
- Stewart, C. R. et al. CD36 ligands promote sterile inflammation through assembly of a Toll-like receptor 4 and 6 heterodimer. *Nature Immunol.* **11**, 155–161 (2010).
- den Dekker, W. K., Cheng, C., Pasterkamp, G. & Duckers, H. J. Toll like receptor 4 in atherosclerosis and plaque destabilization. *Atherosclerosis* **209**, 314–320 (2010).
- Romero-Sandoval, E. A., Horvath, R. J. & DeLeo, J. A. Neuroimmune interactions and pain: focus on glial-modulating targets. *Curr. Opin. Investig. Drugs* **9**, 726–734 (2008).
- O'Neill, L. A. & Bowie, A. G. The family of five: TIR-domain-containing adaptors in Toll-like receptor signalling. *Nature Rev. Immunol.* **7**, 353–364 (2007).
- Dinarello, C. A. Interleukin-1, interleukin-1 receptors and interleukin-1 receptor antagonist. *Int. Rev. Immunol.* **16**, 457–499 (1998).
- Kawai, T. et al. Unresponsiveness of MyD88-deficient mice to endotoxin. *Immunity* **11**, 115–122 (1999).
- Dunne, A. & O'Neill, L. A. The interleukin-1 receptor/Toll-like receptor superfamily: signal transduction during inflammation and host defense. *Sci. STKE* **2003**, re3 (2003).
- Bowie, A. & O'Neill, L. A. The interleukin-1 receptor/Toll-like receptor superfamily: signal generators for pro-inflammatory interleukins and microbial products. *J. Leukoc. Biol.* **67**, 508–514 (2000).
- Beutler, B. et al. Genetic analysis of host resistance: Toll-like receptor signaling and immunity at large. *Annu. Rev. Immunol.* **24**, 353–389 (2006).
- Kobayashi, K. et al. IRAK-M is a negative regulator of Toll-like receptor signaling. *Cell* **110**, 191–202 (2002).
- Suzuki, N. et al. Severe impairment of interleukin-1 and Toll-like receptor signalling in mice lacking IRAK-4. *Nature* **416**, 750–756 (2002).
- Kawagoe, T. et al. Sequential control of Toll-like receptor-dependent responses by IRAK1 and IRAK2. *Nature Immunol.* **9**, 684–691 (2008).
- Wan, Y. et al. Interleukin-1 receptor-associated kinase 2 is critical for lipopolysaccharide-mediated post-transcriptional control. *J. Biol. Chem.* **284**, 10367–10375 (2009).
- Picard, C. et al. Pyogenic bacterial infections in humans with IRAK-4 deficiency. *Science* **299**, 2076–2079 (2003).
- von Bernuth, H. et al. Pyogenic bacterial infections in humans with MyD88 deficiency. *Science* **321**, 691–696 (2008).
- Lasker, M. V., Gajjar, M. M. & Nair, S. K. Cutting edge: Molecular structure of the IL-1R-associated kinase-4 death domain and its implications for TLR signaling. *J. Immunol.* **175**, 4175–4179 (2005).
- Motshwene, P. G. et al. An oligomeric signaling platform formed by the Toll-like receptor signal transducers MyD88 and IRAK-4. *J. Biol. Chem.* **284**, 25404–25411 (2009).
- Park, H. H. et al. The death domain superfamily in intracellular signaling of apoptosis and inflammation. *Annu. Rev. Immunol.* **25**, 561–586 (2007).
- Burns, K. et al. Inhibition of interleukin 1 receptor/Toll-like receptor signaling through the alternatively spliced, short form of MyD88 is due to its failure to recruit IRAK-4. *J. Exp. Med.* **197**, 263–268 (2003).
- Janssens, S. et al. MyD88<sub>s</sub>, a splice variant of MyD88, differentially modulates NF-κB- and AP-1-dependent gene expression. *FEBS Lett.* **548**, 103–107 (2003).
- Loiarro, M. et al. Identification of critical residues of the MyD88 death domain involved in the recruitment of downstream kinases. *J. Biol. Chem.* **284**, 28093–28103 (2009).
- Lawrence, M. C. & Colman, P. M. Shape complementarity at protein/protein interfaces. *J. Mol. Biol.* **234**, 946–950 (1993).
- Li, S., Strelow, A., Fontana, E. J. & Wesche, H. IRAK-4: a novel member of the IRAK family with the properties of an IRAK-kinase. *Proc. Natl Acad. Sci. USA* **99**, 5567–5572 (2002).
- Szabo, G., Dolganiuc, A., Dai, Q. & Pruetz, S. B. TLR4, ethanol, and lipid rafts: a new mechanism of ethanol action with implications for other receptor-mediated effects. *J. Immunol.* **178**, 1243–1249 (2007).
- Rao, N., Nguyen, S., Ngo, K. & Fung-Leung, W. P. A novel splice variant of interleukin-1 receptor (IL-1R)-associated kinase 1 plays a negative regulatory role in Toll/IL-1R-induced inflammatory signaling. *Mol. Cell. Biol.* **25**, 6521–6532 (2005).
- Hardy, M. P. & O'Neill, L. A. The murine *Irak2* gene encodes four alternatively spliced isoforms, two of which are inhibitory. *J. Biol. Chem.* **279**, 27699–27708 (2004).
- Conze, D. B. et al. Lys63-linked polyubiquitination of IRAK-1 is required for interleukin-1 receptor- and toll-like receptor-mediated NF-κB activation. *Mol. Cell. Biol.* **28**, 3538–3547 (2008).
- Cao, Z. et al. TRAF6 is a signal transducer for interleukin-1. *Nature* **383**, 443–446 (1996).
- Belvin, M. P. & Anderson, K. V. A conserved signaling pathway: the *Drosophila* Toll-Dorsal pathway. *Annu. Rev. Cell Dev. Biol.* **12**, 393–416 (1996).
- Sun, H., Bristow, B. N., Qu, G. & Wasserman, S. A. A heterotrimeric death domain complex in Toll signaling. *Proc. Natl Acad. Sci. USA* **99**, 12871–12876 (2002).
- Towb, P., Huaiyu, S. & Wasserman, S. A. Tube is an IRAK-4 homolog in a Toll pathway adapted for development and immunity. *J. Innate Immun.* **1**, 309–321 (2009).
- Holm, L. & Sander, C. Dali: a network tool for protein structure comparison. *Trends Biochem. Sci.* **20**, 478–480 (1995).
- Moncrieffe, M. C., Grossmann, J. G. & Gay, N. J. Assembly of oligomeric death domain complexes during Toll receptor signaling. *J. Biol. Chem.* **283**, 33447–33454 (2008).
- Xiao, T., Towb, P., Wasserman, S. A. & Sprang, S. R. Three-dimensional structure of a complex between the death domains of Pelle and Tube. *Cell* **99**, 545–555 (1999).
- Sun, H. et al. Regulated assembly of the Toll signaling complex drives *Drosophila* dorsoventral patterning. *EMBO J.* **23**, 100–110 (2004).
- Park, H. H. et al. Death domain assembly mechanism revealed by crystal structure of the oligomeric PIDDosome core complex. *Cell* **128**, 533–546 (2007).
- Egelman, E. H. Single-particle reconstruction from EM images of helical filaments. *Curr. Opin. Struct. Biol.* **17**, 556–561 (2007).

**Supplementary Information** is linked to the online version of the paper at [www.nature.com/nature](http://www.nature.com/nature).

**Acknowledgements** We thank K. Rajashankar, I. Kourinov and N. Sukumar for data collection and X. Ma for help with the manuscript. This work was supported by NIH (H.W.), the Cancer Research Institute (S.-C.L. and Y.-C.L.), and the American Heart Association (Y.-C.L.).

**Author Contributions** H.W. initiated the project idea. S.-C.L. and Y.-C.L. designed and performed the experiments. S.-C.L. and H.W. interpreted the data and wrote the manuscript.

**Author Information** The atomic coordinates and structure factors have been deposited in the Protein Data Bank under accession code 3MOP. Reprints and permissions information is available at [www.nature.com/reprints](http://www.nature.com/reprints). The authors declare no competing financial interests. Readers are welcome to comment on the online version of this article at [www.nature.com/nature](http://www.nature.com/nature). Correspondence and requests for materials should be addressed to H.W. ([haowu@med.cornell.edu](mailto:haowu@med.cornell.edu)).

## METHODS

**Protein expression, purification and crystallization.** The DDs of human MyD88 (residues 20–117), IRAK4 (residues 4–106) and IRAK2 (residues 1–112) were co-expressed in *Escherichia coli*. Both MyD88 and IRAK4 DDs were fused to a C-terminal His-tag. The MyD88–IRAK4–IRAK2 complex was purified by Ni-NTA affinity resin and Superdex 200 gel filtration chromatography. The protein concentration for crystallization is about 1 mg ml<sup>-1</sup>. Crystals appeared at 20 °C in hanging drops in conditions of 50 mM Tris at pH 8.0, 100–250 mM MgCl<sub>2</sub>, and 8–15% ethanol. The MyD88–IRAK4 complex was co-expressed in *E. coli* with the exact same constructs except that the IRAK2 gene was not included. The complex was purified with the same method described above. For mutagenesis, all tagged or non-tagged proteins were expressed similarly. To obtain sufficient amount of soluble MyD88 for analysis, a longer MyD88 construct containing residues 20–154 (MyD88-long) was used for expression. To distinguish the IRAK2 band from the MyD88-long and IRAK4 bands on SDS-PAGE, the non-tag version of IRAK2 was fused to two ubiquitins at the N terminus.

**Mutational analysis of complex formation *in vitro*.** Site-directed mutagenesis was performed using the QuikChange kit. All mutations were done on the tagged protein and were confirmed by DNA sequencing. For the co-expression constructs and the His-tagged constructs, the expressed proteins were mixed with the resin and washed three times with 60 mM imidazole. The resin was then mixed with non-tagged protein lysates at room temperature for 1 h, and then washed again three times with 60 mM imidazole. The samples were eluted with 200 mM imidazole and subjected to SDS-PAGE. The gels were stained with Coomassie blue. The complex formation was determined by the ability of the mutant proteins to pull-down other DDs.

**Structure determination and model building.** Diffraction data sets were collected at the X29 and X25 beamlines of NSLS and the 24-ID-E beamline of APS, and processed using HKL2000 (ref. 51). To obtain initial phases, extensive heavy

atom screenings were done with gold, mercury, platinum and tantalum compounds and selenomethione-substituted crystals were obtained. Phases for initial model building were obtained by multiple isomorphous replacement using the program SOLVE<sup>52</sup>, with one gold, two mercury, one platinum, one selenium, and one tantalum derivatives. The electron density was modified and extended by the program RESOLVE<sup>52</sup>. With heavy atom positions and the expected structural homology between the three DDs, six MyD88, four IRAK4, and four IRAK2 molecules can be identified and built accurately. There is one ternary Myddosome complex per crystallographic asymmetric unit with a solvent content of ~72%. The models were subjected to repeated rounds of building with Coot<sup>53</sup> and refinement with CNS<sup>54</sup>. The model was also subjected to translation/libration/screw vibrational motion refinement by the program Phenix<sup>55</sup>. Residues 94–112 of IRAK2 were not visible in the electron density maps. The structure was analysed using the CCP4 suite<sup>56</sup>, the ProtorP server<sup>57</sup>, and the Dali server<sup>45</sup>. All figures were made using PyMOL<sup>58</sup>.

51. Otwinowski, Z. & Minor, W. Processing of X-ray diffraction data collected in oscillation mode. *Methods Enzymol.* **276**, 307–326 (1997).
52. Terwilliger, T. SOLVE and RESOLVE: automated structure solution, density modification and model building. *J. Synchrotron Radiat.* **11**, 49–52 (2004).
53. Emsley, P. & Cowtan, K. Coot: model-building tools for molecular graphics. *Acta Crystallogr. D* **60**, 2126–2132 (2004).
54. Brunger, A. T. *et al.* Crystallography & NMR system: a new software suite for macromolecular structure determination. *Acta Crystallogr. D* **54**, 905–921 (1998).
55. Adams, P. D. *et al.* PHENIX: building new software for automated crystallographic structure determination. *Acta Crystallogr. D* **58**, 1948–1954 (2002).
56. Collaborative Computational Project. The CCP4 suite: programs for protein crystallography. *Acta Crystallogr. D* **50**, 760–763 (1994).
57. Reynolds, C., Damerell, D. & Jones, S. ProtorP: a protein–protein interaction analysis server. *Bioinformatics* **25**, 413–414 (2009).
58. Delano, W. L. The PyMol Molecular Graphics System (<http://www.pymol.org/>) (2002).



**Supplementary Table 1.** Crystallographic statistics

	Native	Se-Met	Ta <sub>6</sub> Br <sub>12</sub> <sup>2+</sup>	K <sub>2</sub> PtBr <sub>4</sub>	C <sub>2</sub> H <sub>5</sub> HgCl
<b>Data collection</b>	NSLS X29	NSLS X29	NSLS X29	NSLS X29	NSLS X25
Wavelength (Å)	1.0750	0.9768	1.2547	1.0716	1.0057
Space group	C222 <sub>1</sub>	C222 <sub>1</sub>	C222 <sub>1</sub>	C222 <sub>1</sub>	C222 <sub>1</sub>
Cell dimensions (Å)	101.7, 307.1, 187.6	100.6, 305.4, 188.5	101.8, 306.8, 187.8	101.5, 307.2, 189.5	103.1, 304.4, 188.4
Resolution (Å)	30 - 3.4	35 - 7.5	30 - 4.5	50 - 6.5	30 - 7.2
R <sub>sym</sub> (%)	7.8 (50.6)	7.4 (39.7)	5.0 (49.4)	4.5 (43.3)	5.1 (33.1)
I / σI	17.4 (1.9)	11.0 (4.0)	13.0 (1.8)	19.3 (4.6)	18.0 (5.6)
Completeness (%)	97.4 (81.8)	99.9 (100.0)	98.9 (90.9)	98.7 (99.4)	100.0 (100.0)
Redundancy	9.4 (5.2)	4.7 (4.7)	4.6 (3.6)	5.1 (5.1)	5.0 (5.2)
Sites found		7	12	17	12
Mean Figure of Merit	0.64				
<b>Refinement</b>				KAu(CN) <sub>2</sub>	(C <sub>2</sub> H <sub>5</sub> HgO)HPO <sub>2</sub>
Resolution (Å)	20 - 3.4			<b>Data collection</b>	APS 24-ID-E
No. reflections	33,422			Wavelength (Å)	0.9792
R <sub>work</sub> / R <sub>free</sub> (%)	21.6 / 26.1			Space group	C222 <sub>1</sub>
No. atoms	11,548			Cell dimensions (Å)	101.6, 307.2, 187.1
Average B-factors (Å <sup>2</sup> )	180.0			Resolution (Å)	30 - 7.0
R.m.s deviations				R <sub>sym</sub> (%)	7.1 (45.8)
Bond lengths / angles	0.012 Å / 1.59 °			I / σI	10.1 (2.5)
Ramachandran plot				Completeness (%)	99.6 (99.9)
Most favored / allowed	69.9 % / 99.6 %			Redundancy	3.9 (4.0)
				Sites found	14
					8

†Highest resolution shell is shown in parenthesis.

**Supplementary Table 2.** Number of observed Se-sites in the anomalous difference Fourier

Se-site	Predict*	M <sup>1</sup>	M <sup>2</sup>	M <sup>3</sup>	M <sup>4</sup>	M <sup>5</sup>	M <sup>6</sup>	I4 <sup>1</sup>	I4 <sup>2</sup>	I4 <sup>3</sup>	I4 <sup>4</sup>	I2 <sup>1</sup>	I2 <sup>2</sup>	I2 <sup>3</sup>	I2 <sup>4</sup>
MyD88	2	1	1	2	2	2	2	0	-	-	-	-	-	-	-
IRAK4	0	-	-	-	-	-	-	0	0	0	0	0	-	-	-
IRAK2	4	-	-	-	-	-	-	-	-	-	-	4	4	4	3

\*The first Met residues were excluded.

**Supplementary Table 3.** Pairwise superposition among MyD88 DD, IRAK4 DD and IRAK2 DD, with PIDD DD and RAIDD DD, and with the isolated IRAK4 DD

	IRAK4	IRAK2	PIDD	RAIDD	IRAK4 (2a9i)*
MyD88	77 C $\alpha$ , 1.22 Å	74 C $\alpha$ , 1.29 Å	62 C $\alpha$ , 1.60 Å	56 C $\alpha$ , 1.46 Å	
IRAK4		82 C $\alpha$ , 1.16Å	52 C $\alpha$ , 1.49 Å	59 C $\alpha$ , 1.52 Å	105 C $\alpha$ , 0.70 Å
IRAK2			54 C $\alpha$ , 1.52 Å	53 C $\alpha$ , 1.57 Å	

\*Structure of IRAK4 DD in isolation.

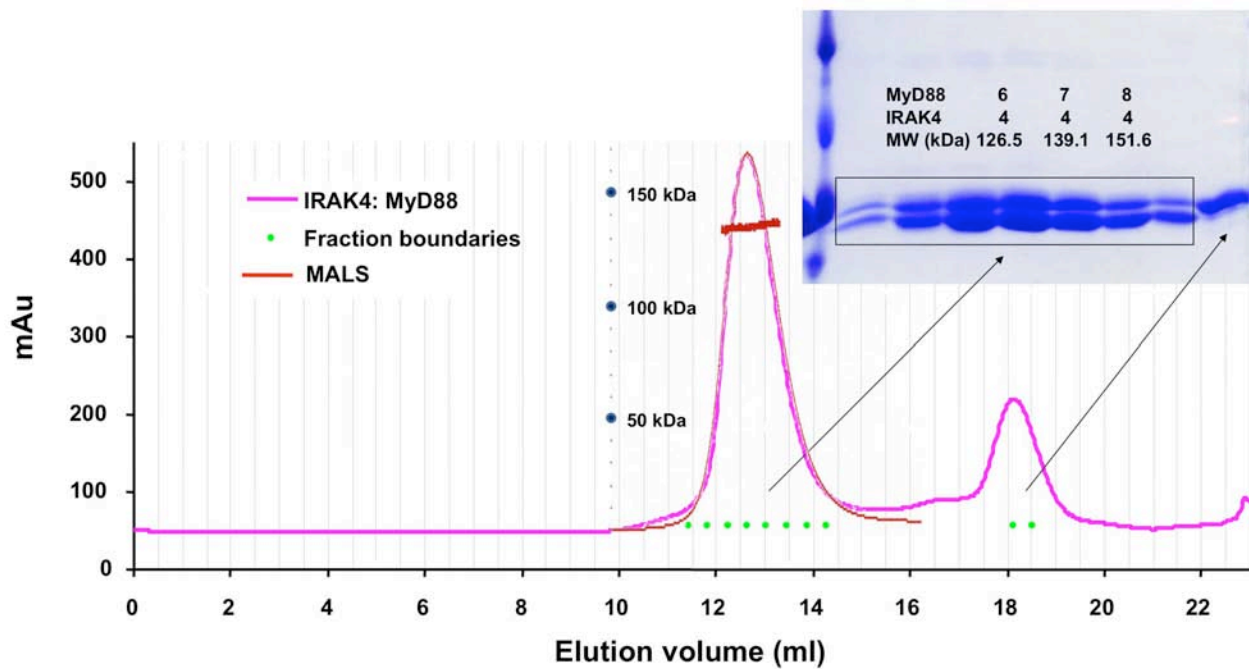
**Supplementary Table 4.** Structural homology search using the DALI server\*

	Top match			Second match		
	Name	PDB	Z-score	Name	PDB	Z-score
MyD88	UNC5H2	1wmg	11.4	IRAK4	2a9i	11.2
IRAK4	Tube	1d2z	13.8	Pelle	1d2z	12.9
IRAK2	Pelle	1d2z	13.6	IRAK4	2a9i	12.7

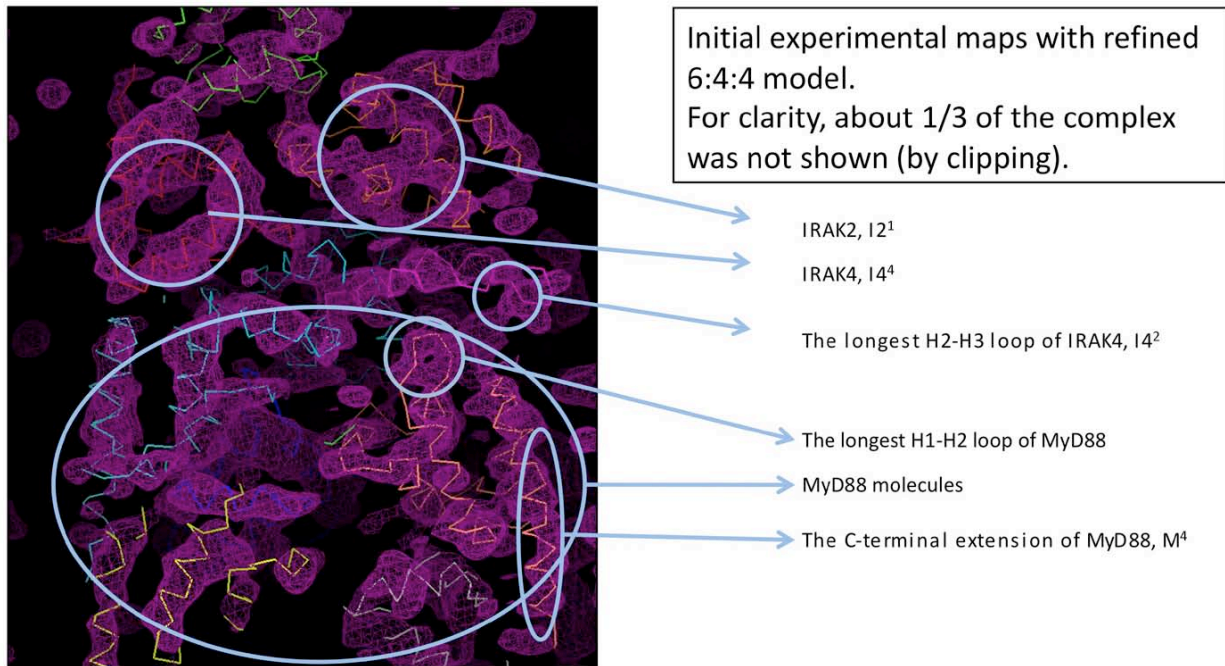
\*Holm, L. and Sander, C., Dali: a network tool for protein structure comparison. *Trends Biochem. Sci.* **20**, 478 (1995).



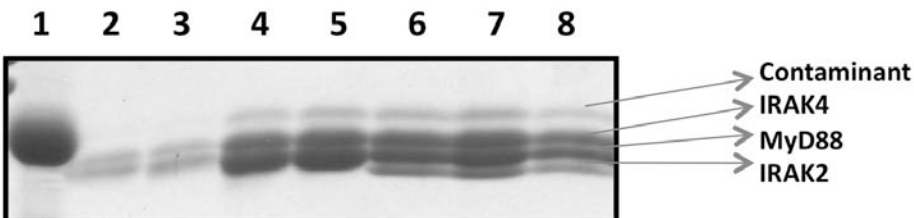
**Supplementary Figure 1.** The gel filtration profile and the MALS measurement of the MyD88: IRAK4 DD complex. The calculated molecular mass for 6: 4, 7: 4 or 8: 4 stoichiometry of the MyD88: IRAK4 complex is shown. A molecular mass of 135.4 kDa (0.5% error) was obtained, which could best represent a 7:4 stoichiometry with a calculated molecular mass of 139.1 kDa. However, it is most likely that the gel filtration peak contains complexes of variable stoichiometry with an average molecular mass of ~135 kDa, including the major species of 7: 4 and 8: 4 complexes and the 6: 4 complex observed under a mild stripping mass spectrometry condition (Motshwene, P. G. et al., An oligomeric signaling platform formed by the Toll-like receptor signal transducers MyD88 and IRAK-4. *J Biol Chem* 284 (37), 25404 (2009)). In the crystal, both 7: 4 and 8: 4 complexes can be accommodated without causing steric hindrance in crystal packing. No additional MyD88 molecules were observed probably due to their lower occupancies in the crystal. The SDS-PAGE shows the two gel filtration peaks; upper band is IRAK4 and the lower band is MyD88.



**Supplementary Figure 2.** Experimental electron density map superimposed with the final atomic model



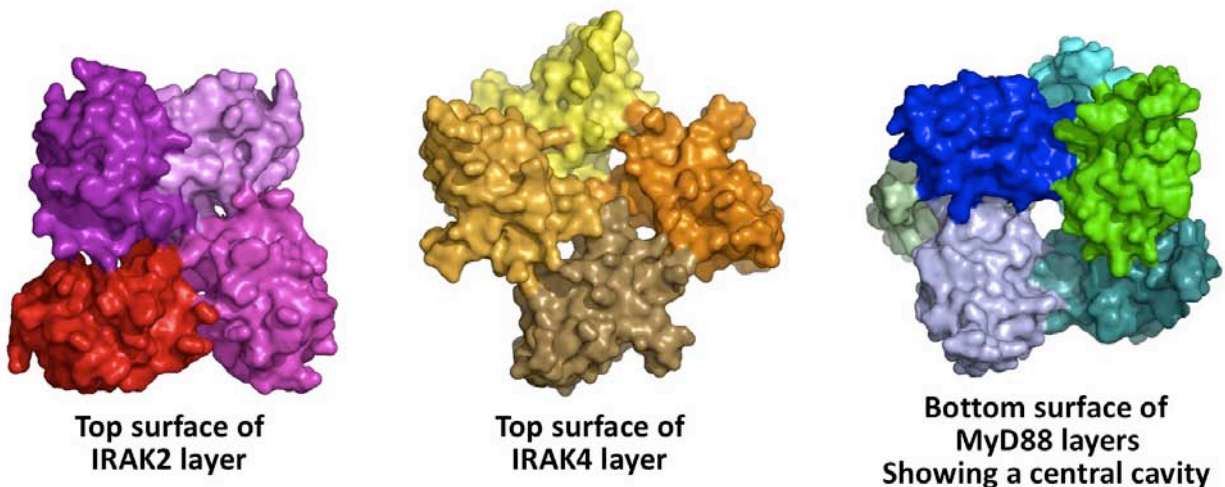
**Supplementary Figure 3.** SDS-PAGE of the MyD88: IRAK4 binary and the MyD88: IRAK4: IRAK2 ternary complexes



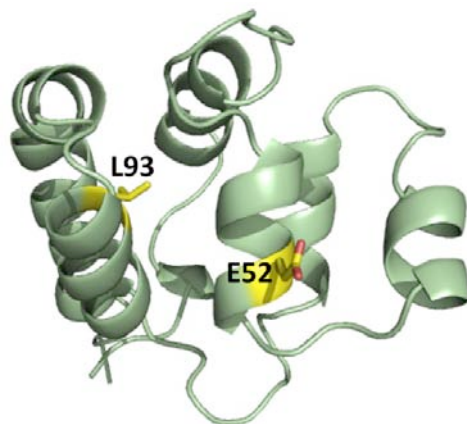
1. LMW marker of 14kDa.
2. MyD88: IRAK4 complex (diluted)
3. MyD88: IRAK4 complex (diluted, different fractions)
4. MyD88: IRAK4 complex
5. MyD88: IRAK4 complex (different fractions)
6. MyD88: IRAK4: IRAK2 complex
7. MyD88: IRAK4: IRAK2 complex (different fractions)
8. MyD88: IRAK4: IRAK2 complex (different fractions)



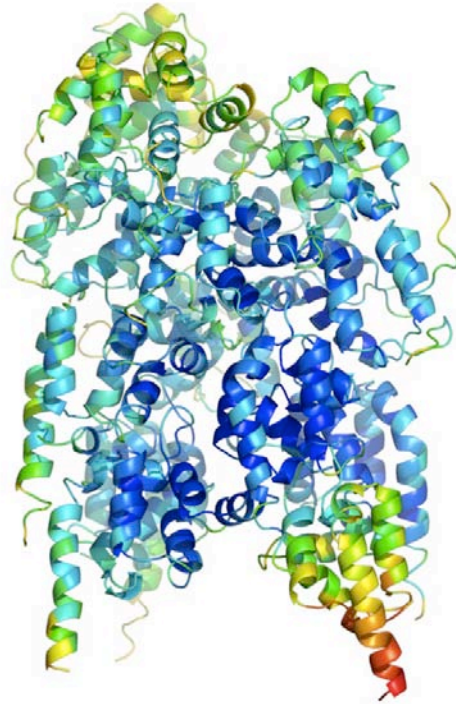
**Supplementary Figure 4.** Surface diagrams of each of the layers. The size of the central cavity in the MyD88 layers has an estimated diameter of  $\sim 15$  Å at the widest part and a depth of  $\sim 35$  Å.



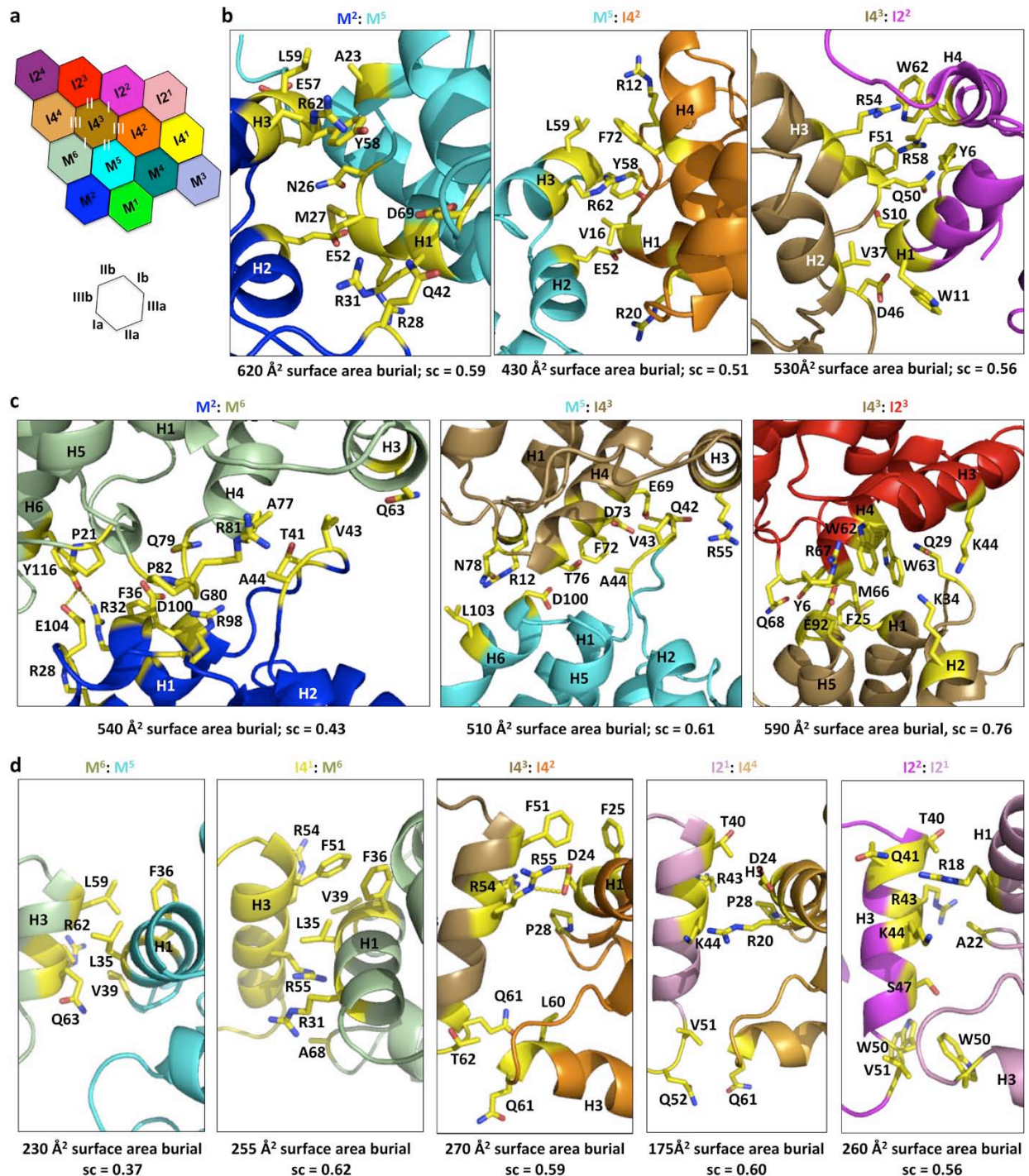
**Supplementary Figure 5.** Two human disease mutations of MyD88,  $\Delta E52$  and L93P, map to the H2 and H5 helices of the DD, respectively. The  $\Delta E52$  mutation would have changed the register of residues on the helix and disrupt the folding. Because L93 side chain is buried, the L93P mutation will not only affect the helix formation but also hydrophobic core of the DD.



**Supplementary Figure 6.** Temperature factor distribution in the ternary complex using rainbow colors with low temperature factors in the blue end and high temperature factors in the red end of the spectrum.

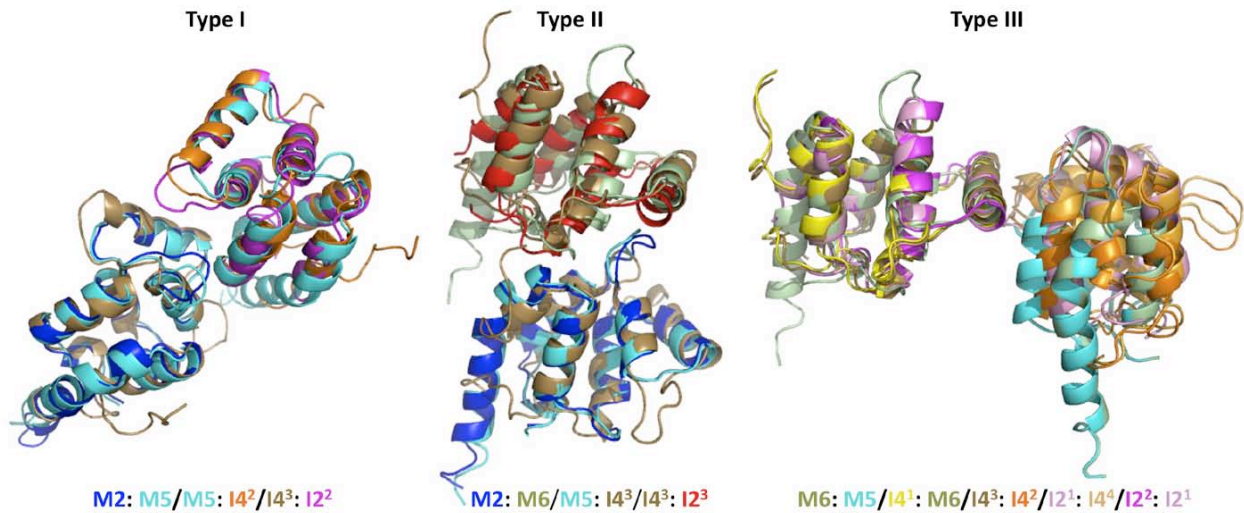


**Supplementary Figure 7.** Detailed interactions in the ternary complex. Buried surface areas and shape complementarity (sc) scores are shown. Side chains are labeled. Molecules are shown in the same color coding as in Fig. 1a. a, A schematic diagram showing the three types of interactions in the complex. b, The three type I interactions in the complex, MyD88: MyD88, MyD88: IRAK4 and IRAK4: IRAK2. c, The three type II interactions in the complex, MyD88: MyD88, MyD88: IRAK4 and IRAK4: IRAK2. d, The five type III interactions in the complex, MyD88: MyD88, MyD88: IRAK4, IRAK4: IRAK4, IRAK4: IRAK2 and IRAK2: IRAK2.





**Supplementary Figure 8.** Superpositions of the three type I interactions, the three type II interactions and the five type III interactions in the ternary complex. Ribbon diagrams of the superpositions are shown at the top panel. The RMSDs and the number of superimposed C $\alpha$  atoms are shown at the lower panel. For comparison, the RMSDs and the number of superimposed C $\alpha$  atoms are also shown for the PIDD:RAIDD complex.

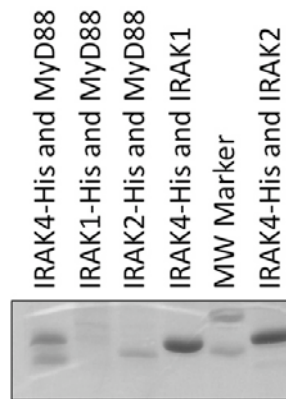


<b>MyD88:IRAK4:IRAK2</b>											
Surface type	I			II			III				
Pairs	M2:M5	M5:I4 <sup>2</sup>	I4 <sup>3</sup> :I2 <sup>2</sup>	M2:M6	M5:I4 <sup>3</sup>	I4 <sup>3</sup> :I2 <sup>3</sup>	M6:M5	I4 <sup>1</sup> :M6	I4 <sup>3</sup> :I4 <sup>2</sup>	I2 <sup>1</sup> :I4 <sup>4</sup>	I2 <sup>2</sup> :I2 <sup>1</sup>
RMSD (Å)	Ref	1.4	1.8	Ref	1.4	1.9	Ref	1.1	1.7	2.1	2.3
# Atoms		183	162		181	162		181	157	163	164
RMSD (Å)		Ref	1.6		Ref	1.6		Ref	1.1	1.5	1.9
# Atoms			166			167			183	162	171
RMSD (Å)								Ref	0.9	1.4	
# Atoms										192	171
RMSD (Å)									Ref	0.9	
# Atoms											178
<b>PIDD:RAIDD</b>											
Surface type	I			II			III				
Pairs	P5:P1	P1:R2	R5:R1	R1:P1	R6:R5		P1:P2	R5:P1	R4:R5		
RMSD (Å)	Ref	1.6	2.0	Ref	1.7		Ref	1.3	2.4		
# Atoms		178	161		170			166	160		
RMSD (Å)		Ref	1.4					Ref	1.6		
# Atoms			166								170

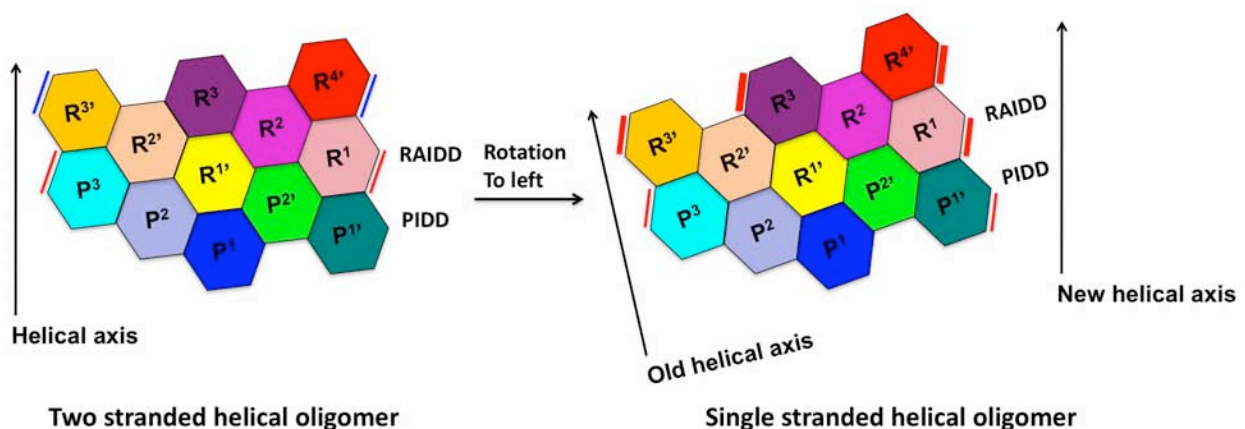
Ref: reference molecule



**Supplementary Figure 10.** Pairwise co-expression experiments among MyD88, IRAK1, IRAK2 and IRAK4



**Supplementary Figure 11.** Relationship between double-stranded helical symmetry and single-stranded helical symmetry in a schematic diagram. The 5 PIDD (P): 7 RAIDD (R) complex is used as an example. In the left panel, the interaction surfaces of adjacent DDs in the first and second helical strands are labeled with red and blue lines, respectively. These red or blue lines should align at the same height along the helical axis. In the right panel, the adjacent DDs in the single helical strand are labeled with red lines of the same widths. In the left panel, the two adjacent DDs skip a “notch” so that two helices co-exist in the complex. The two helices are  $P^1, P^2, P^3, R^1, R^2, R^3$  and  $P^{1'}, P^{2'}, R^{1'}, R^{2'}, R^{3'}$ . In the right panel, the assembly is rotated to the left to become less steep along the helical axis so that  $P^3$  is connected to  $P^{1'}$  in a single helical symmetry. The single helix would have the order of  $P^1, P^2, P^3, P^{1'}, P^{2'}, R^{1'}, R^{2'}, R^{3'}, R^1, R^2, R^3, R^{4'}$ .





### **Supplementary Discussion 1. Stoichiometry of the complex in solution and in the crystal**

Previous nano-electrospray ionization mass spectra of a MyD88: IRAK4 DD complex acquired under conditions that preserve non-covalent interactions showed a major species with a stoichiometry of 7:4 and a second species with a stoichiometry of 8:4<sup>1</sup>. At higher activation energies, stoichiometries of 6:4, 7:3, and 8:3 "stripped complexes" after ejection of single subunits were observed following gas phase dissociation events<sup>1</sup>. Our multi-angle light scattering (MALS) measurement of the MyD88: IRAK4 complex gave a molecular mass of 135.4 kDa (0.5% error) (Supplementary Fig. 1), which could best represent a 7:4 stoichiometry with a calculated molecular mass of 139.1 kDa. However, it is most likely that the complex contains populations of variable stoichiometries with an average molecular mass of ~135 kDa, possibly including but not limited to 7:4, 8:4 and 6:4 complexes. On a molecular level, this variable stoichiometry of MyD88 may be contributed by its uniquely long H1-H2 loop, which inserts between two adjacent MyD88 molecules, making MyD88 self-assembly possible. In the crystal, both 7:4 and 8:4 complexes with one and two additional MyD88 molecules, respectively, can be accommodated without causing steric hindrance in crystal packing. No additional MyD88 molecules were observed probably due to their lower occupancies in the crystal.

- 1 Motshwene, P. G. et al., An oligomeric signaling platform formed by the Toll-like receptor signal transducers MyD88 and IRAK-4. *J Biol Chem* **284** (37), 25404 (2009).

### **Supplementary Discussion 2. Cooperativity in the assembly of the complex**

Assembly of the MyD88: IRAK4 and the MyD88: IRAK4: IRAK2 complexes should both be highly cooperative given the involvement of multiple subunits in the process. This cooperativity implies that formation of the complex has a steep dependence on receptor-mediated clustering of MyD88 and on concentrations of the component proteins in the cell. This high dependence ensures that assembly of the complex and induction of signaling are tightly regulated.